İSTANBUL TECHNICAL UNIVERSITY ★ INSTITUTE OF SCIENCE AND TECHNOLOGY

BURIED OBJECT APPROACH FOR SOLVING ELECTROMAGNETIC SCATTERING PROBLEMS INVOLVING ROUGH SURFACES

Ph.D. Thesis by
Yasemin ALTUNCU, M.Sc.

Department : Electronic and Communication Engineering
Programme: Electronic and Communication Engineering

APRIL 2006

İSTANBUL TECHNICAL UNIVERSITY ★ INSTITUTE OF SCIENCE AND TECHNOLOGY

BURIED OBJECT APPROACH FOR SOLVING ELECTROMAGNETIC SCATTERING PROBLEMS INVOLVING ROUGH SURFACES

Ph.D. Thesis by
Yasemin ALTUNCU, M.Sc.
(504002210)

Date of submission : 29 December 2005

Date of defence examination: 19 April 2006

Supervisor (Chairman): Prof. Dr. İbrahim AKDUMAN

Members of the Examining Committee: Prof. Dr. Ercan TOPUZ (I.T.U)

Prof.Dr. Gökhan UZGÖREN (I.K.U)

Prof.Dr. Tayfun GÜNEL (I.T.U)

Prof.Dr. M. İrşadi AKSUN (Koç Uni.)

APRIL 2006

İSTANBUL TEKNİK ÜNİVERSİTESİ ★ FEN BİLİMLERİ ENSTİTÜSÜ

DÜZGÜN OLMAYAN YÜZEYLERİ İÇEREN ELEKTROMAGNETİK SAÇILMA PROBLEMLERİNİN ÇÖZÜMÜ İÇİN GÖMÜLÜ CİSİM YAKLAŞIMI

DOKTORA TEZİ

Y. Müh. Yasemin ALTUNCU
(504002210)

Tezin Enstitüye Verildiği Tarih : 29 Aralık 2005
Tezin Savunulduğu Tarih : 19 Nisan 2006

Tez Danışmanı : Prof. Dr. İbrahim AKDUMAN

Diğer Jüri Üyeleri: Prof. Dr. Ercan TOPUZ (İ.T.Ü)

Prof.Dr. Gökhan UZGÖREN (İ.K.Ü)

Prof.Dr. Tayfun GÜNEL (İ.T.Ü)

Prof.Dr. M. İrşadi AKSUN (Koç Üni.)

NİSAN 2006

ACKNOWLEDGEMENT

I would like to express my immense gratitude to Prof. Dr. İbrahim AKDUMAN who gave me the opportunity to do research under his supervision for his precious guidance and supports during this study. I would also like to deeply thank to Assoc. Prof. Dr. Ali YAPAR for his great help and many valuable contributions to this thesis.

April-2006 Yasemin ALTUNCU

TABLE OF CONTENTS

Page No:

LIST OF ABBREVIATIONS iv

LIST OF FIGURES v

LIST OF SYMBOLS vi

SUMMARY vii

ÖZET ix

1 INTRODUCTION 1

1.1 Scattering from Rough Surfaces 1

1.2 Scattering from Objects Buried Under a Rough Surface . 2

1.3 The Aim of the Work 4

2 SCATTERING OF ELECTROMAGNETIC WAVES FROM A HALF-SPACE WITH ROUGH SURFACE 7

2.1 Formulation of the Scattering Problem 7

2.2 Buried Object Representation 9

2.3 Green's Function of the Two-Part Space with Planar Interface 12

2.4 A Numerical Solution for the Integral Equation 14

2.5 Near and Far Field Expressions of Scattered Wave 16

3 SCATTERING OF ELECTROMAGNETIC WAVES BY BODIES BURIED IN A HALF-SPACE WITH ROUGH SURFACE 20

3.1 Formulation of the Scattering Problem 20

3.2 Green's Function of Two Half-Space Medium with Rough Interface 23

3.3 Far Field Expression of the Scattered Wave 25

4 NUMERICAL IMPLEMENTATION 27

4.1 Numerical Results for Scattering from Rough Surface . . 27

4.2 **Numerical Results for Scattering from Objects Buried under a Rough Surface** 35

5 CONCLUSIONS **44**

REFERENCES **46**

BIOGRAPHY **52**

LIST OF ABBREVIATIONS

MoM : Method of Moment
RCS : Radar cross-section
BOA : Buried object approach
RMS : Root mean square

LIST OF FIGURES

Page No:

2.1 Geometry of the scattering problem related to rough surface . . . 8

2.2 Buried object modelling of the rough interface 9

2.3 Geometry for the field u_0 10

2.4 Regularity line of $\hat{G}_0$ in the complex ν-plane. 13

2.5 Mapping of C_R in the complex α-plane. 17

3.1 Geometry of the scattering problem related to buried object . . . 21

4.1 Variation of $|u_s|$ versus x_1/λ on the plane $x_2 = 2\lambda$ for a sinusoidal rough surface. 28

4.2 Comparison of the average coherent scattering cross-sections of the buried object approach and the small perturbation method after 150 realizations 28

4.3 SW(σ_{2D}) versus observation angle ϕ for the surfaces having different rms heights and correlation lengths. 29

4.4 Variation of the amplitude of the total field for a smoothly varying air-dry soil interface. 30

4.5 Variation of the amplitude of the total field for a random air-dry soil interface with $\sigma_r = 0.3\lambda, \ell_c = 0.2\lambda, L = 4\lambda$. 31

4.6 Variation of the amplitude of the total field for a random air-dry soil interface with $\sigma_r = 0.2\lambda, \ell_c = 0.2\lambda, L = 4\lambda$. 32

4.7 Variation of the amplitude of the total field for a random air-wet soil interface with $\sigma_r = 0.2\lambda, \ell_c = 0.2\lambda, L = 4\lambda$. 32

4.8 Variation of the amplitude of the total field for a random air-mica interface with $\sigma_r = 0.2\lambda, \ell_c = 0.6\lambda, L = 7\lambda$ and $\phi_0 = \pi/2$. 33

4.9 Variation of the amplitude of the total field for a random air-mica interface with $\sigma_r = 0.2\lambda, \ell_c = 0.6\lambda, L = 7\lambda$ and $\phi_0 = \pi/4$. 33

4.10 Variation of the amplitude of the total field for a random air-sea interface with $\sigma_r = 0.4\lambda, \ell_c = 0.5\lambda, L = 10\lambda$. 34

4.11 Comparison of the scattering widths due to a circular cylinder buried under a flat and sinusoidal rough interfaces. 36

4.12 Scattering widths values corresponding three different object configurations buried under a random surface with $\sigma_r = 0.4\lambda, \ell_c = 0.3\lambda$ and $L = 6\lambda$. 37

4.13 Scattering widths corresponding to buried circular cylinder in the existence of three different levels of the roughness. 38

4.14 Scattering widths corresponding three different conductivities of the buried object. 38

4.15 Scattering widths corresponding three different incidence angles of the plane wave. 39

4.16 The magnitude of the total electric field in the existence of two concentric circular cylinders buried beneath (a) a flat air-dry soil surface and (b) a random rough surface of $\sigma_r = 0.3\lambda, \ell_c = 0.4\lambda$ and $L = 5\lambda$ 40

4.17 The magnitude of the total electric field in the existence of elliptical objects with same cross-sections, buried under a random rough interface with $\sigma_r = 0.4\lambda, \ell_c = 0.3\lambda$ and $L = 18\lambda$ 41

4.18 The magnitude of the total electric field in the existence of a rectangular object buried under a random and highly rough surface with $\sigma_r = 2.2\lambda, \ell_c = 0.3\lambda$ and $L = 10\lambda$ 42

4.19 The magnitude of the total electric field in the existence of three different shaped objects having different conductivities buried under a rough interface with $\sigma_r = 0.4\lambda, \ell_c = 0.5\lambda$ and $L = 8\lambda$ 43

LIST OF SYMBOLS

$\vec{E}$: Electric field vector
μ_0 : Permeability of the free space
ε_1 : Dielectric permittivity of the upper half space
ε_2 : Dielectric permittivity of the lower half space
σ_1 : Conductivity of the upper half space
σ_2 : Conductivity of the lower half space
k_1 : Wavenumber of the upper half space
k_2 : Wavenumber of the lower half space
ω : Angular frequency
λ : Wavelength
ϕ_0 : Incidence angle
χ : Transmission angle
R : Reflection coefficient
T : Transmission coefficient
u_i : Incident field
u_0 : Total field in absence of rough surface
u_s : Scattered field from the rough surface
u : Total field in absence of buried object
$\tilde{u}_s$: Scattered field from buried object
$\tilde{u}$: Total field
G_0 : Green's function of the two part space with planar interface
$\hat{G}_0$: Fourier transform of G_0
$\bar{G}$: Green's function of the two part space with rough interface
G_s : Contribution of the rough surface to the Green's function of the two part space media with rough interface
υ : Object function for the buried bodies
υ_R : Object function for the rough surface
σ_r : Rms height
ℓ_c : Correlation length
σ_{2D} : Scattering width
Γ : Interface of two half spaces
δ : Dirac delta distribution

BURIED OBJECT APPROACH FOR SOLVING ELECTROMAGNETIC SCATTERING PROBLEMS INVOLVING ROUGH SURFACES

SUMMARY

In this thesis, a novel and effective method is presented for the solution of two classes of electromagnetic scattering problems, i.e.: for the scattering from a half-space having rough surface and for the scattering from objects buried under a rough surface. Such problems are of great importance in electromagnetic theory due to the their potential applications in practice such as modeling of ground wave propagation, remote sensing of geophysical terrains such as snow, soil and vegetation, detection and location of dielectric mines, non-destructive testing, determination of underground cracks and earthquake zones, detection of underground tunnels and pipelines etc.

First a method is given for the solution of scattering problems from a rough interface between two lossy dielectric half-spaces in the case of plane wave illumination. For the sake of simplicity we consider one dimensional locally rough surfaces. In our approach we account for the scattering from the irregularities of the rough surface as scattering from objects buried in two half-spaces separated by a planar interface. This allows us to formulate the problem as a scattering problem related to cylindrical bodies of arbitrary cross sections. Through the Green's function of the two half-spaces medium where the irregularities are buried, the problem is reduced to the solution of a Fredholm integral equation of second kind which can be treated by using one of the known techniques. In this work, we solved the integral equation via an application of Method of Moments (MoM) by reducing it to a linear system of equations. The computational cost of the present method is directly proportional to the number of irregularities of the surface and their sizes. As a result the method is very effective for surfaces having a localized roughness, arbitrary rms height and slope. The method permits us to obtain both near and far field expressions of the scattered wave in the half-spaces above and below the surface.

The *buried object approach* to a rough surface allows us also to solve the scattering problems related to the bodies buried under a rough surface. In this work we consider cylindrical bodies buried under a one dimensional locally rough surface and illuminated by a time harmonic plane wave. Through the Green's function of the background medium with rough interface the problem is reduced to the solution of a Fredholm integral equation of the second kind for the scattered field due to the bodies, which is solved here via application of MoM. On the other hand the determination of the Green's function constitutes a separate and difficult problem in the case of two half-spaces characterized by different media

and separated by a rough interface. This can be done by solving the scattering problem from rough interface in the case of line source illumination through the *buried object approach* (BOA) described above. The present method permits us to obtain both near and far field expressions of the scattered wave for buried objects of arbitrary number and shapes.

We here compared our numerical results results with those given in the open literature. It has been observed that our approach yields quite accurate results, and furthermore it provides a region of validity which is wider than the available methods.

DÜZGÜN OLMAYAN YÜZEYLERİ İÇEREN ELEKTROMAGNETİK SAÇILMA PROBLEMLERİNİN ÇÖZÜMÜ İÇİN GÖMÜLÜ CİSİM YAKLAŞIMI

ÖZET

Bu tez çalışmasında, engebeli yüzeye sahip bir yarı uzaydan saçılma ve engebeli yüzey altına gömülü cisimlerden saçılma problemleri olmak üzere iki tür elektromagnetik saçılma probleminin çözümü için yeni ve etkin bir yöntem verilmiştir. Söz konusu problemler, yer dalgası yayılımının modellenmesi, kar, toprak ve bitki örtüsü gibi yer yüzeyinin jeofiziksel özelliklerinin uzaktan algılanması, dielektrik mayınların tespiti, tahribatsız muayene, yer kabuğu altındaki çatlak ve fayların bulunması, yer altındaki tünel ve boru hatlarının belirlenmesi gibi pek çok uygulama alanına sahip olmaları sebebiyle elektromagnetik teoride büyük öneme sahiptirler.

İlk olarak, düzlemsel dalga ile aydınlatma durumunda, kayıplı iki dielektrik yarı uzay arasındaki engebeli arayüzeye ilişkin saçılma problemlerinin çözümü için bir yöntem verilmiştir. Basitlik açısından bir boyutlu engebeli yüzeyler gözönüne alınmıştır. Bizim yaklaşımımızda, düzgün olmayan yüzeyin engebeleri, düzlemsel arayüzeye sahip iki parçalı uzaya gömülü cisimler olarak kabul edilmekte ve bu da problemi, rastgele kesitlere sahip silindirik cisimlere ilişkin saçılma problemi gibi düzenlemeye olanak vermektedir. Engebelerin gömülü olduğu iki parçalı uzayın Green fonksiyonu aracılığıyla problem ikinci tip bir Fredholm integral denkleminin çözümüne indirgenmekte olup bu denklem bilinen sayısal teknikler kullanılarak çözülebilmektedir. Bu çalışmada, integral denklem, bir lineer denklem sistemine dönüştürülerek Moment yöntemiyle (MoM) çözülmüştür. Verilen yöntemin hesaplama maliyeti doğrudan yüzeyin engebelerinin sayısına ve büyüklüğüne bağlıdır. Sonuç olarak yöntem, lokal bir aralıkta herhangi bir karesel ortalama (rms) yüksekliğe ve eğime sahip olan engebelerden oluşan yüzeyler için oldukça etkindir. Yöntem, yüzeyin altındaki ve yüzeyin üstündeki yarı uzaylarda saçılan alanın hem uzak alan hem de yakın alan ifadelerinin elde edilmesine müsade etmektedir.

Engebeli yüzeye, gömülü cisimler gibi yaklaşmak, engebeli yüzey altına gömülü cisimlere ilişkin saçılma problemlerinin çözümüne de olanak sağlamaktadır. Bu amaçla, düzlemsel dalga ile aydınlatılan, bir boyutlu, lokal bir aralıkta engebelere sahip olan bir yüzey altına gömülü silindirik cisimler gözönüne alınmıştır. Engebeli arayüzeye sahip iki parçalı uzayın Green fonksiyonu yardımıyla, cisimlerden saçılan alan problemi, ikinci tip bir Fredholm integral denklemine dönüştürülmüş ve MoM kullanılarak çözülmüştür. Diğer taraftan, arayüzeyi engebeli iki parçalı uzayın Green fonksiyonunun belirlenmesi ayrı ve zor bir problem oluşturmaktadır. Bu problemin çözümü, yukarıda bahsedilen gömülü cisim yaklaşımıyla, çizgisel

kaynakla aydınlatma durumu için engebeli arayüzeyden saçılma problemini çözülerek yapılır. Verilen yöntem, herhangi bir sayıda ve herhangi bir şekle sahip olan cisimler için saçılan dalganın uzak ve yakın alan ifadelerini elde etmeye imkan vermektedir.

Elde edilen yöntem, heriki problem için de literatürde verilen sonuçlarla karşılaştırılmak suretiyle test edilmiştir. Yöntemin oldukça iyi sonuçlar verdiği gözlenmiştir. Yöntemin geçerlilik aralığı uygulanabilen diğer yöntemlere göre daha yüksektir.

1 INTRODUCTION

Analysis of electromagnetic scattering both by rough surfaces and by objects buried in a layered media with rough interfaces constitute an important and interesting class of problems in electromagnetic theory due to their applications in practice. In the investigation of scattering problems related to rough surfaces one tries to investigate the affects of rough surfaces on the propagation of electromagnetic waves. On the other hand scattering from objects buried in a layered media with rough interfaces is a more complex problem and in most cases it also involves the analysis of scattering from rough surfaces. The objective of this thesis is to give a new and efficient method for the solution of both kind of problems. In the sequel of this chapter we first give a detailed review of available methods for both cases and then present an introductory explanation of the new proposed methods.

1.1 Scattering from Rough Surfaces

Electromagnetic scattering problems related to rough surfaces have applications in modeling of ground wave propagation, remote sensing of geophysical terrains such as snow, soil and vegetation etc. For example the effect of complex rough structure of earth surface on the propagation of electromagnetic waves can be exploited by considering appropriate models and solving the related scattering problems. According to the frequency of the electromagnetic wave, earth surface can be modeled as a perfectly conducting rough surface, or it can be considered as a rough interface between two dielectric media. In both cases efficient and accurate solutions are necessary for deep understanding of the scattering phenomena from rough surfaces.

During the past five decades enormous efforts have been devoted in the investigation of scattering from rough surfaces in various areas such as electromagnetic,

acoustics, optics etc. and several analytical and numerical techniques have been developed. Most of the developed methods are based on the use of perturbation theories and physical optic approximations [1, 2]. However they are restricted in domain of validity. For surfaces with small surface root mean square (rms) height and slope the small perturbation method is the most commonly used formalism in the low frequency region. This method involves a perturbation series in surface height for scattered field. Then by using either Rayleigh hypothesis or extended boundary condition the expansion coefficients are obtained recursively. The small perturbation method is mostly used for scattering from dielectric and perfectly conducting rough surfaces [3]-[6]. The Kirchhoff approximation which is nothing but an application of physical optic theory for high frequency region is used when the surface inhomogeneities relatively have small slope and large radii of curvature. In this approach the surface fields at a given point are approximated by those of the local tangent plane [7, 8]. Much works have been done to conduct the theories which extend the range of validity of the rough surface parameters beyond the conventional Kirchhoff and perturbation theories; phase perturbation method, unified perturbation method and integral equation method are the most common ones of these techniques [9]-[15]. In particular, for 1-D surfaces, surface based-integral methods yield extremely efficient solutions for the backscattered field from rough surfaces [16]. On the other hand, in the application of such methods it is required to truncate the scattering surface which causes numerical errors in the solution for the surface fields near the truncation points and in some circumstances may eliminate important contributions to the scattered field [17]. In order to reduce end effect errors, a tapered incident field is frequently used which restricts to use surface based integral methods for the plane, cylindrical or spherical wave incidences. Different type of approaches has also been investigated by several researchers [18]-[21]. A very detailed review of the studies and the validity regions of the conventional methods is given in [22]-[24].

1.2 Scattering from Objects Buried Under a Rough Surface

As is mentioned above the investigation of electromagnetic scattering by objects buried in a layered medium is of importance since they have various applications in practice in the areas such as detection and location dielectric mines, non-destructive testing, determination of underground cracks and earthquake zones, detection of underground tunnels an pipelines etc. Although these applications are recognized as an "inverse scattering problem" in electromagnetic theory, the solutions of the related direct scattering problems make a valuable contribution to overcome difficulties which may occur in the investigation of inversion algorithms. For example, several difficulties arise in the determination of dielectric mines due to the clutters and low penetration of RF signal into the moist soil. Most of these difficulties might be simplified with a deep understanding of the nature of scattering from such buried objects. Although during the last three decades several exact and numerical techniques have been developed, a large number of them are related to the layered backgrounds with planar boundaries [25]-[28]. Whereas in most of the real applications the bodies are buried in layered media having rough interfaces and the roughness have a strong effect on the scattering phenomena. For instance, in the case of bodies buried underground the roughness of the earth surface can potentially modify object scattering returns from those with a flat surface. For that reason the problem has to be considered in its actual conditions. In other words one has to take into consideration the roughness of the interfaces between the layers where the body is located. Such kind of problems gained considerable attention during the last three decades. In [29, 30] the scattering from a circular cylinder buried under a sinusoidal interface is treated by using an integral equation combined with the extended boundary condition approach. An analytical solution for a buried circular cylinder beneath a slightly rough surface is given in [31]. In this study all of the multiple interactions between the body and the rough surface are accounted for in the solution by the use of small perturbation approach. Some other approximate analytical solutions in the small roughness limit are presented in [32, 33]. On the other hand scattering from three dimensional (3-D) bodies buried under a two-dimensional (2-D) rough interface are considered a different category from 2-D

scattering from cylindrical objects. They are more complex, CPU and memory demanding problems and one can find many publications related to this topic which we mention only some of them here. Among the numerical studies the most recent ones are [34]-[37]. In [34, 35] scattering from 3-D objects buried under a two-dimensional rough interface is presented. The method is similar to one that is used in the study for the perfectly conducting bodies [37] and is based on an iterative Method of Moments (MoM) solution. The method is valid for moderate surface roughness and object sizes compared to the wavelength. A hybrid method which combines the analytical methods and numerical algorithms is given in [36]. Scattering from multiple 3-D objects buried under a 2-D slightly rough interface is analyzed by steepest descent fast multi-pole method in [38, 39]. It should be noted that for 2-D scattering problems from cylindrical objects buried under a rough surface several methods based on MoM have been developed for the highly rough surfaces [40]. In [40] a surface integral method based on a generalization of the extinction theorem to multiple connected domains is presented for the case of Gaussian beam illumination. We note that surface based integral methods applied to scattering problems involving rough surfaces require to truncate the rough surface which causes numerical errors in the solution for the surface fields near the truncation points and in some circumstances may eliminate important contributions to the scattered field [17]. In order to reduce end effect errors, a tapered or localized (Gaussian beam for example as in [40]) field is frequently used which restricts to use surface based integral methods for

1.3 The Aim of the Work

Although the above mentioned studies have made a valuable contribution to the subjects described above there is need for alternative approaches capable of extending the range of validity of available methods and also providing better computational efficiencies. The main objective of this thesis is to give a new and efficient method for the solution of the two-classes of problems explained in Section 1.2 and Section 1.3.

a) The first aim of the thesis is to give a new and efficient method for the solution of scattering problems related to rough interfaces between two lossy dielectric

half-spaces in the case of plane wave illumination. For the sake of simplicity we consider one dimensional locally rough surfaces. In our approach we consider the irregularities of the rough surface as buried objects in a two half-spaces media with planar interface which allows us to formulate the problem as a scattering problem related to cylindrical bodies of arbitrary cross sections. Through the Green's function of the two half-spaces medium where the irregularities are buried, the problem is reduced to the solution of a Fredholm integral equation of second kind which can be treated by using one of the known techniques. In this study, we solved the integral equation via an application of Method of Moments (MoM) by reducing it to a linear system of equations. Modeling the rough surface in terms of a volumetric domain was considered earlier in 3-D by other researchers [41, 42]. In those studies the rough interface is assumed to be the boundary of an infinite layer and then the scattering problem is formulated as a scattering of electromagnetic waves from this infinite volumetric domain. On the contrary in the present approach the surface is represented in terms of finite number of bounded scatterers. The computational cost of the present method is directly proportional to the number of irregularities of the surface and their sizes. As a result the method is very effective for surfaces having a localized roughness, arbitrary rms height and slope. The method permits us to obtain both the near and far field expressions of the scattered wave in the half-spaces above and below the surface. We have shown that the results of the method match with those obtained through the existing ones.

b) Scattering from bodies buried in a half-space with rough interface will also be considered in this thesis. To this aim it will be considered cylindrical bodies buried under a one dimensional locally rough interface. The material of the bodies are assumed to be inhomogeneous, i.e: their dielectric permittivities and conductivities are the functions of location. Through the Green's function of the background medium with rough interface the problem is reduced to the solution of a Fredholm integral equation of the second kind for the scattered field due to the bodies, which is solved here by an application of MoM. On the other hand the determination of the Green's function constitutes a separate and difficult problem in the case of two half-spaces medium with rough interface. In the open

literature not much work has been done in that direction except [43], which is valid only for the slightly rough surfaces. Whereas the method developed here for the scattering from rough interfaces can also be used to obtain the required Green's function. This can be done by just solving the scattering problem from rough interface in the case of line source illumination through the *buried object approach* (BOA) described above [44, 45]. The computational cost of the Green's function is directly proportional to the number of irregularities of the surface and their sizes. As a result the method is very effective for surfaces having a localized roughness, arbitrary rms height and slope. Note that the locality limitation of the surface is to guarantee to have finite number of objects in the evaluation of the Green's function. In the surface based integral methods which gives effective solutions for highly rough surfaces this is done by using tapered or localized incident waves. The present method permits us to obtain both near and far field expressions of the scattered wave for buried objects of arbitrary number and shapes. We compare our results with those given in [31] and it has been observed that both results match. The maximum level of roughness in the numerical examples is chosen as comparable to those given in [40] but it can be higher in general.

The organization of the thesis is as follows: In Section 2 a new method based on the *buried object approach* for the scattering of electromagnetic waves from a locally rough surface is given. In Section 3 the scattering problem related to cylindrical bodies of arbitrary materials and cross-sections buried beneath a rough interface is solved using *buried object approach*. Numerical results are given in Section 4 and a conclusion is presented in Section 5. A time factor $e^{-i\omega t}$ is assumed and omitted throughout the thesis.

2 SCATTERING OF ELECTROMAGNETIC WAVES FROM A HALF-SPACE WITH ROUGH SURFACE

In this section we will give a numerical method for the scattering of electromagnetic waves from rough surfaces separating two lossy dielectric half-spaces. It is first given a general formulation of the scattering problem and then a new approach which is called *buried object approach* is presented. A numerical solution based on Method of Moments, which is very efficient for calculating near and far field scattered fields, is derived through the Green's function of two-part space medium with planar boundary.

2.1 Formulation of the Scattering Problem

The geometry of the problem illustrated in Figure 2.1. In this configuration the whole space is separated into two half-spaces by the interface Γ which is defined by the relation $x_2 = f(x_1)$ where $f(x_1)$ is a single valued function [46]. Γ is assumed to be locally rough, i.e.: $f(x_1)$ differs from the planar surface over a finite interval whose length is L. Γ can also be a random surface, in that case, it is represented by the parameters rms height σ_r, correlation length ℓ_c for a given correlation function. A detailed procedure of the random rough surface generation is given in [47]. The regions $x_2 > f(x_1)$ and $x_2 < f(x_1)$ are assumed to be filled with non-magnetic simple materials having dielectric permittivities and conductivities ε_1, σ_1 and ε_2, σ_2, respectively.

The scattering problem considered here is to determine the effect of Γ on the propagation of electromagnetic waves excited in the upper half-space $x_2 > f(x_1)$, more precisely to obtain the scattered field from the surface Γ. To this aim the half-space $x_2 < f(x_1)$ is illuminated by a time-harmonic plane wave whose electric field vector is always parallel to the Ox_3 axis, namely,

$$\vec{E}_i = (0, 0, u_i(x_1, x_2)) \tag{2.1}$$

$$u_i(x_1, x_2) = e^{-ik_1(x_1 \cos\phi_0 + x_2 \sin\phi_0)} \tag{2.2}$$

where $\phi_0 \in (0, \pi)$ is the incidence angle while k_1 stands for the wave number of the upper half-space which is defined by the square root of $k_1^2 = w^2\varepsilon_1\mu_0 + iw\sigma_1\mu_0$.

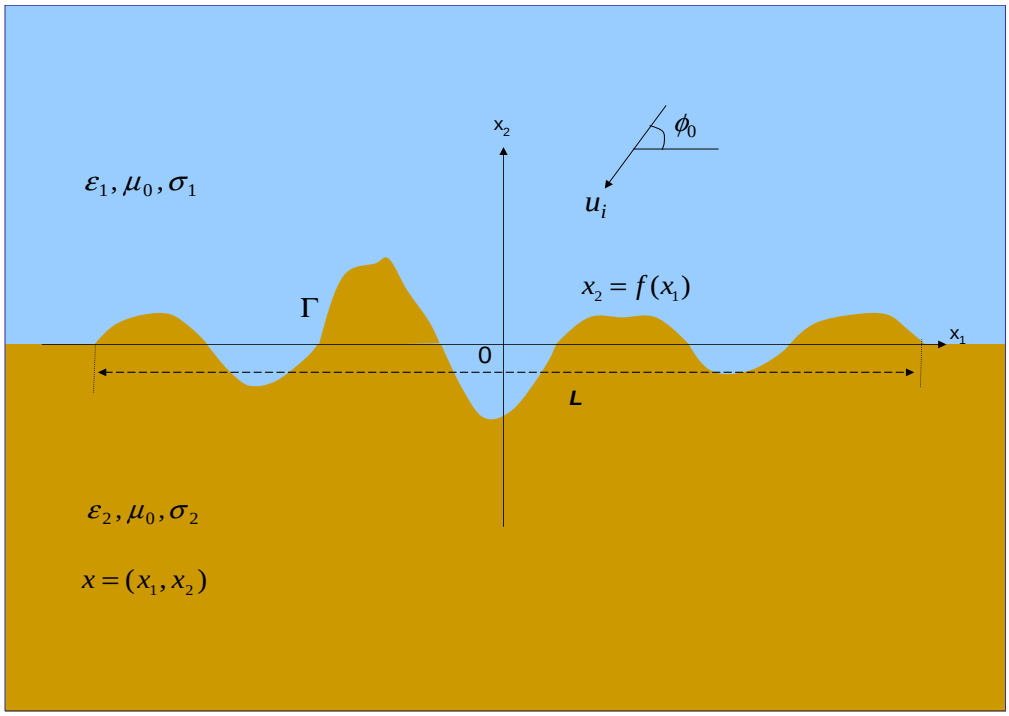


Figure 2.1: Geometry of the scattering problem related to rough surface

Since the problem is homogeneous in the Ox_3 direction, the total electric field vector will also be parallel to the Ox_3-axis, namely, $\vec{E} = (0, 0, u(\mathbf{x}))$, where $\mathbf{x} = (x_1, x_2)$ denotes the position vector in $\mathbb{R}^2$. Thus the problem is reduced to a scalar one in terms of the total field function $u(\mathbf{x})$ which satisfies the reduced wave equation

$$\triangle u + k^2(\mathbf{x})u = 0 \tag{2.3}$$

in the sense of distribution [48] and under the appropriate radiation condition for $|\mathbf{x}| \to \infty$. In (2.3)

$$k^2(\mathbf{x}) = \begin{cases} k_1^2, & x_2 > f(x_1) \\ \\ k_2^2, & x_2 < f(x_1) \end{cases} \tag{2.4}$$

stands for the square of the wave-number of the two-part space with $k_2^2 = w^2\varepsilon_2\mu_0 + iw\sigma_2\mu_0$. The scattering problem is then to obtain the total electric field $u(\mathbf{x})$, in other words to solve (2.3) for a given $k^2(\mathbf{x})$ and Γ.

2.2 Buried Object Representation

In order to solve the scattering problem described in the previous section we first assume that the whole space is separated into two parts by the plane $x_2 = 0$. Then the half-spaces $x_2 > 0$ and $x_2 < 0$ contain 2N finite domains bounded by Γ and $x_2 = 0$ plane as shown in Figure 2.2. The ones in the region $x_2 > 0$ are denoted by $D_1, D_3, ..., D_{2N-1}$ and the rest in the $x_2 < 0$ by $D_2, D_4, ..., D_{2N}$. Note that the dielectric permittivities and conductivities of the regions $D_n, n = 1, 3, ...2N - 1$ and $D_n, n = 2, 4, ...2N$ are ε_2, σ_2 and ε_1, σ_1, respectively.

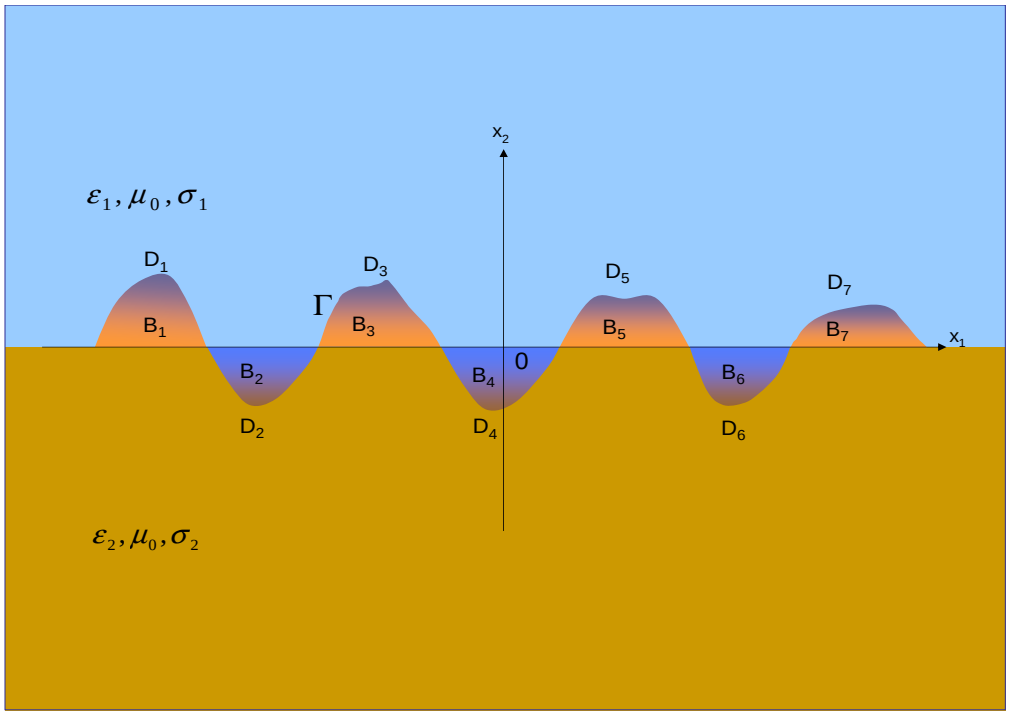


Figure 2.2: Buried object modelling of the rough interface

Then the regions $D_1, D_2, ..., D_{2N}$ can be considered as buried cylindrical bodies whose cross-sections with the Ox_1x_2 plane are $B_1, B_2, ..., B_{2N}$, respectively, into two half-spaces medium with the planar interface at $x_2 = 0$. In other words, with this approach the scattering problem is reduced to the solution of the problems connected with the scattering of plane electromagnetic waves from 2N homoge-

neous objects buried in a two-part space medium having a planar interface.

In order to formulate the problem more easily consider now the field $u_0(\mathbf{x})$ which would be created by the incident field (2.1) in the case of two-half spaces medium separated by the plane $x_2 = 0$ (See Figure 2.3).

This field satisfies

$$\triangle u_0 + k^2(x_2)u_0 = 0 \tag{2.5}$$

where $k^2(x_2)$ stands for the wave number related to the two-part space in Figure 2.3; namely,

$$k^2(x_2) = \begin{cases} k_1^2, & x_2 > 0 \\ \\ k_2^2, & x_2 < 0 \end{cases} . \tag{2.6}$$

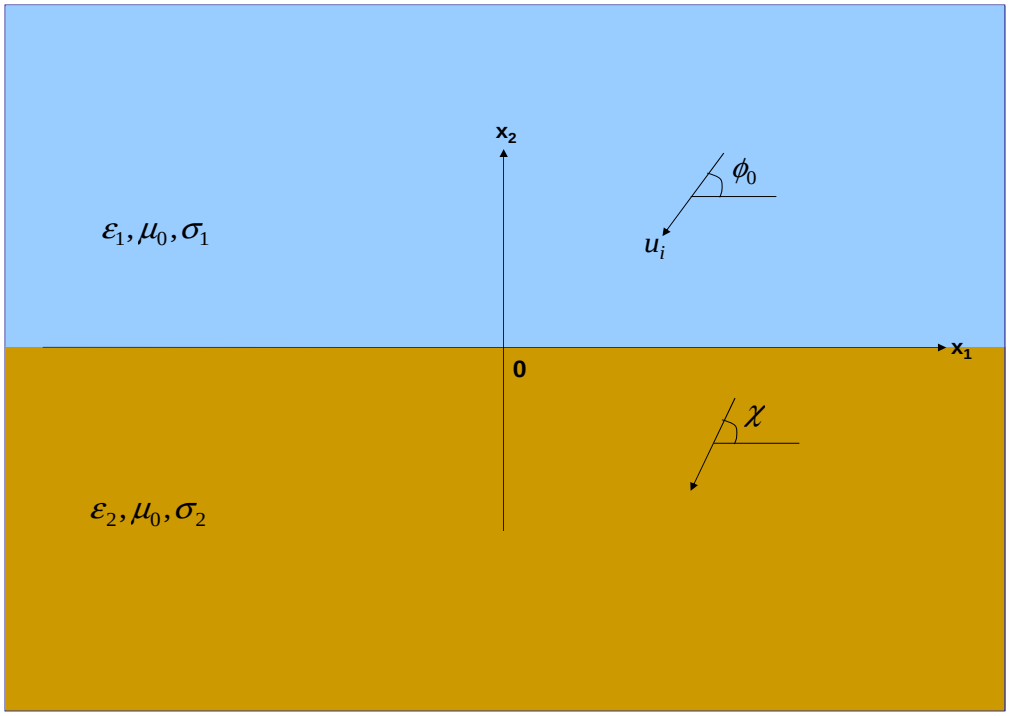


Figure 2.3: Geometry for the field u_0

The solution of (2.5) is very straightforward and it can be found in any ordinary textbook and, one has

$$u_0(\mathbf{x}) = \begin{cases} u_i(\mathbf{x}) + Re^{-ik_1(x_1\cos\phi_0 - x_2\sin\phi_0)}, & x_2 > 0 \\ \\ Te^{-ik_2(x_1\cos\chi + x_2\sin\chi)}, & x_2 < 0 \end{cases} \tag{2.7}$$

where χ is the transmission angle given by the Snell's law

$$k_1\cos\phi_0 = k_2\cos\chi \tag{2.8}$$

while R and T are the reflection and transmission coefficients of the plane $x_2 = 0$,

$$R = \frac{k_1\sin\phi_0 - k_2\sin\chi}{k_1\sin\phi_0 + k_2\sin\chi} \tag{2.9}$$

$$T = \frac{2k_1\sin\phi_0}{k_1\sin\phi_0 + k_2\sin\chi}. \tag{2.10}$$

Hence, the contribution of the regions $D_1, D_2, ..., D_{2N}$ to the total field, say $u_s(\mathbf{x})$, consists in the difference

$$u_s(\mathbf{x}) = u(\mathbf{x}) - u_0(\mathbf{x}) \tag{2.11}$$

and satisfies the reduced wave equation

$$\triangle u_s(\mathbf{x}) + k^2(x_2)u_s(\mathbf{x}) = -k^2(x_2)\upsilon_R(\mathbf{x})u(\mathbf{x}) \tag{2.12}$$

in the sense of distribution under the radiation condition for $|\mathbf{x}| \to \infty$. Here, the function $\upsilon_R(\mathbf{x})$ is the well-known object function related to the regions $D_1, D_2, ..., D_{2N}$ and is given by the relation

$$\upsilon_R(\mathbf{x}) = \begin{cases} \upsilon_1 = \frac{\varepsilon_2}{\varepsilon_1} - 1, & \mathbf{x} \in D_1, D_3, ..., D_{2N-1} \\ \\ \upsilon_2 = \frac{\varepsilon_1}{\varepsilon_2} - 1, & \mathbf{x} \in D_2, D_4, ..., D_{2N} \\ \\ 0, & otherwise. \end{cases} \tag{2.13}$$

Note that the support of the function $\upsilon_R(\mathbf{x})$ is the union of the regions $B_1, B_2, ..., B_{2N}$.

Consider now the Green's function $G_0(\mathbf{x};\mathbf{y})$ of the two-part space with planar interface at $x_2 = 0$. It permits us to convert the differential equation (2.12)

into the following Fredholm integral equation of the second kind which is a more advantageous representation for our purposes:

$$u_s(\mathbf{x}) = k_1^2 \upsilon_1 \sum_{n=1}^{N} \int_{B_{2n-1}} G_0(\mathbf{x};\mathbf{y})(u_0(\mathbf{y}) + u_s(\mathbf{y}))d\mathbf{y} \\ + k_2^2 \upsilon_2 \sum_{n=1}^{N} \int_{B_{2n}} G_0(\mathbf{x};\mathbf{y})(u_0(\mathbf{y}) + u_s(\mathbf{y}))d\mathbf{y}. \tag{2.14}$$

In Section 2.4 a method based on the MoM will be given to solve $u_s(\mathbf{x})$ from (2.14). Before going further, it will be convenient to give an explicit expression of the Green's function $G_0(\mathbf{x};\mathbf{y})$.

2.3 Green's Function of the Two-Part Space with Planar Interface

By definition the Green's function $G_0(\mathbf{x};\mathbf{y})$ satisfies the equation

$$\triangle G_0(\mathbf{x};\mathbf{y}) + k^2(\mathbf{x}_2)G_0(\mathbf{x};\mathbf{y}) = -\delta(\mathbf{x}-\mathbf{y}) \tag{2.15}$$

in the sense of distributions under the radiation condition. In this equation $\mathbf{y} \in I\!R^2$ is an arbitrary point and δ is the Dirac's delta distribution.

In order to find a suitable expression of G_0, consider first its Fourier transform with respect to x_1, namely,

$$\hat{G}_0(\nu, x_2, ;\mathbf{y}) = \int_{-\infty}^{\infty} G_0(\mathbf{x};\mathbf{y}) e^{-i\nu x_1} dx_1. \tag{2.16}$$

Then the transformations of (2.15) and the boundary conditions at $x_2 = 0$ yield the following problem for $\hat{G}_0$

$$\frac{d^2\hat{G}_0}{dx_2^2} - (\nu^2 - k_j^2)\hat{G}_0 = -e^{-i\nu y_1}\delta(x_2 - y_2),\ j = 1, 2, \quad \nu \in C_R \tag{2.17}$$

$$\hat{G}_0 \quad and \quad \frac{\partial \hat{G}_0}{\partial x_2} \quad are\ \ continuous\ \ on\ \ x_2 = 0 \tag{2.18}$$

$$|\hat{G}_0| \to 0 \ \ as \ \ |\mathbf{x}| \to \infty. \tag{2.19}$$

Here C_R stands for a horizontal straight line in the regularity strip of $\hat{G}_0$ in the complex ν-plane (see Figure 2.4)[49].

After some straightforward calculations and through the well-known inverse transform integral

$$G_0(\mathbf{x};\mathbf{y}) = \frac{1}{2\pi}\int_{C_R} \hat{G}_0(\nu, x_2;\mathbf{y}) e^{i\nu x_1} d\nu \ , \tag{2.20}$$

one can get an explicit expression of $G_0(\mathbf{x};\mathbf{y})$ as follows:

$$G_0(\mathbf{x};\mathbf{y}) = \begin{cases} \frac{i}{4}H_0^{(1)}(k_1|\mathbf{x}-\mathbf{y}|) + G_{0R}^{(1)}(\mathbf{x};\mathbf{y}); & x_2 > 0,\ y_2 > 0 \\ G_{0T}^{(1)}(\mathbf{x};\mathbf{y}); & x_2 < 0,\ y_2 > 0 \\ G_{0T}^{(2)}(\mathbf{x};\mathbf{y}); & x_2 > 0,\ y_2 < 0 \\ \frac{i}{4}H_0^{(1)}(k_2|\mathbf{x}-\mathbf{y}|) + G_{0R}^{(2)}(\mathbf{x};\mathbf{y}); & x_2 < 0,\ y_2 < 0 \end{cases} \tag{2.21}$$

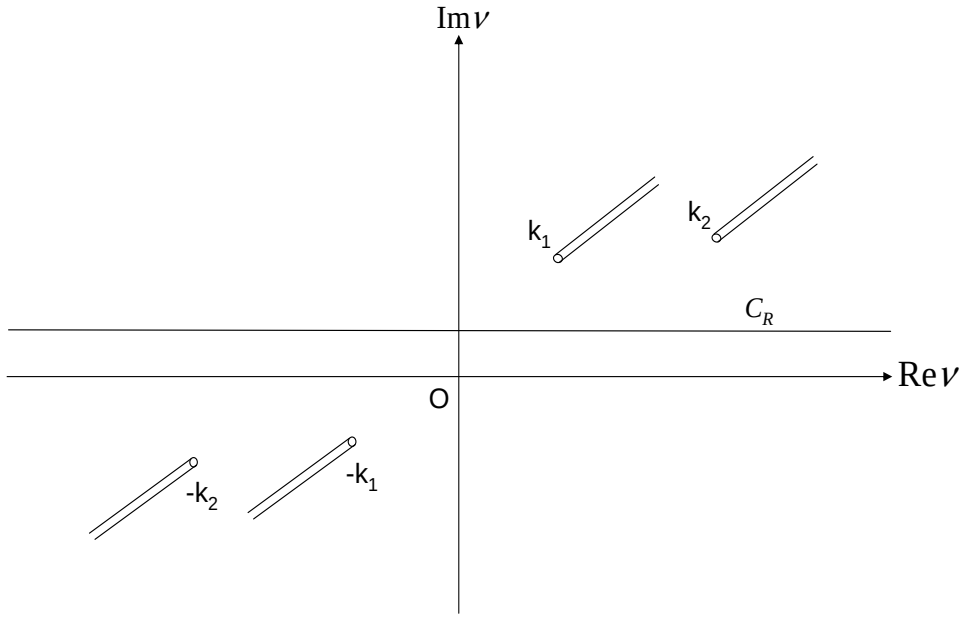


Figure 2.4: Regularity line of $\hat{G}_0$ in the complex ν-plane.

where

$$G_{0R}^{(1)}(\mathbf{x};\mathbf{y}) = \frac{1}{2\pi}\int_{C_R} \frac{1}{2\gamma_1}\frac{\gamma_1-\gamma_2}{\gamma_1+\gamma_2} e^{-\gamma_1(x_2+y_2)} e^{i\nu(x_1-y_1)} d\nu \tag{2.22}$$

$$G_{0T}^{(1)}(\mathbf{x};y) = \frac{1}{2\pi}\int_{C_R} \frac{1}{2\gamma_1}\frac{2\gamma_1}{\gamma_1+\gamma_2} e^{-\gamma_1 y_2+\gamma_2 x_2} e^{i\nu(x_1-y_1)} d\nu \tag{2.23}$$

$$G_{0T}^{(2)}(\mathbf{x};\mathbf{y}) = \frac{1}{2\pi}\int_{C_R}\frac{1}{2\gamma_2}\frac{2\gamma_2}{\gamma_1+\gamma_2}e^{\gamma_2 y_2-\gamma_1 x_2}e^{i\nu(x_1-y_1)}d\nu \tag{2.24}$$

$$G_{0R}^{(2)}(\mathbf{x};\mathbf{y}) = \frac{1}{2\pi}\int_{C_R}\frac{1}{2\gamma_2}\frac{\gamma_2-\gamma_1}{\gamma_1+\gamma_2}e^{\gamma_2(x_2+y_2)}e^{i\nu(x_1-y_1)}d\nu \tag{2.25}$$

while $H_0^{(1)}$ denotes zero order Hankel function of the first kind. In (2.22-2.25) the functions γ_1 and γ_2 stand for the square roots

$$\gamma_1(\nu) = \sqrt{\nu^2-k_1^2}\ , \qquad \gamma_2(\nu) = \sqrt{\nu^2-k_2^2} \tag{2.26}$$

which are defined in the complex ν-plane cut as shown in Figure 2.4 with the conditions [49]

$$\gamma_j(0) = -ik_j\ , \quad j=1,2. \tag{2.27}$$

From (2.22-2.25) and (2.21) we can easily see that G_0 is symmetrical, i.e: $G_0(\mathbf{x},\mathbf{y}) = G_0(\mathbf{y},\mathbf{x})$ and has the property

$$G_0(\mathbf{x},\mathbf{y}) = \tilde{G_0}(|x_1-y_1|,x_2,y_2),\ \ \mathbf{x},\mathbf{y}\in I\!R^2. \tag{2.28}$$

2.4 A Numerical Solution for the Integral Equation

In the sequel we will describe a method which is an application of MoM to solve $u_s(\mathbf{x})$ from (2.14) [50]. To this aim we first write (2.14) in an abbreviated form

$$(I-A)u_s(\mathbf{x}) = \bar{u}(\mathbf{x}),\ \ \mathbf{x}\in I\!R^2 \tag{2.29}$$

where A is the linear operator defined by

$$Au_s(\mathbf{x}) = \sum_{n=1}^{N}[k_1^2\upsilon_1\int_{B_{2n-1}}G_0(\mathbf{x};\mathbf{y})u_s(\mathbf{y})d\mathbf{y} + k_2^2\upsilon_2\int_{B_{2n}}G_0(\mathbf{x};\mathbf{y})u_s(\mathbf{y})d\mathbf{y}] \tag{2.30}$$

while $\bar{u}(\mathbf{x})$ is the known function

$$\bar{u}(\mathbf{x}) = \sum_{n=1}^{N}[k_1^2\upsilon_1\int_{B_{2n-1}}G_0(\mathbf{x};\mathbf{y})u_0(\mathbf{y})d\mathbf{y} + k_2^2\upsilon_2\int_{B_{2n}}G_0(\mathbf{x};\mathbf{y})u_0(\mathbf{y})d\mathbf{y}]. \tag{2.31}$$

Consider now the n'th region B_n and divide it into M_n small cells which allows one to write

$$\int_{B_n} G_0(\mathbf{x};\mathbf{y})u_s(\mathbf{y})d\mathbf{y} = \sum_{m=1}^{M_i} \int_{S_{nm}} G_0(\mathbf{x};\mathbf{y})u_s(\mathbf{y})d\mathbf{y}, \tag{2.32}$$

where S_{nm} denotes m'th cell of the region B_n. If S_{nm} is small enough one can make the approximation $u_s(\mathbf{y}) \simeq u_s(\mathbf{y}^{nm})$ for the scattered field inside the related cell, where $\mathbf{y}^{nm} = (y_1^{nm}, y_2^{nm})$ stands for the center point of the cell S_{nm}. Then one can write

$$\int_{B_n} G_0(\mathbf{x};\mathbf{y})u_s(\mathbf{y})d\mathbf{y} \simeq \sum_{m=1}^{M_n} u_s(\mathbf{y}^{nm})C^{nm}(\mathbf{x}), \tag{2.33}$$

here we put

$$C^{nm}(\mathbf{x}) = \int_{Snm} G_0(\mathbf{x};\mathbf{y})d\mathbf{y}. \tag{2.34}$$

When the geometry of S_{nm} is given one can calculate the coefficients $C_{nm}(\mathbf{x})$ through (2.21) and (2.34). For a rectangular cell with side lengths $2\Delta y_1 \times 2\Delta y_2$, $C^{nm}(\mathbf{x})$ will be

$$C^{nm}(\mathbf{x}) = \begin{cases} C_0^{nm}(\mathbf{x}) + C_1^{nm}(\mathbf{x}); & x_2 > 0,\ y_2^{nm} > 0 \\ C_2^{nm}(\mathbf{x}); & x_2 < 0,\ y_2^{nm} > 0 \\ C_3^{nm}(\mathbf{x}); & x_2 > 0,\ y_2^{nm} < 0 \\ C_4^{nm}(\mathbf{x}) + C_5^{nm}(\mathbf{x}); & x_2 < 0,\ y_2^{nm} < 0 \end{cases} \tag{2.35}$$

where

$$C_0^{nm}(\mathbf{x}) = \begin{cases} \frac{i}{2k_1^2}[\pi k_1 a H_1^{(1)}(k_1 a) + 2i], & n = m \\ \frac{i\pi a}{2k_1} J_1(k_1 a) H_0^{(1)}(k_1|\mathbf{x} - \mathbf{y}^{nm}|) & , n \neq m \end{cases} \tag{2.36}$$

$$C_1^{nm}(\mathbf{x}) = \frac{2}{\pi} \int_{C_R} \frac{1}{2\gamma_1} \frac{\gamma_1 - \gamma_2}{\gamma_1 + \gamma_2} \frac{\sinh(\gamma_1 \Delta \mathbf{y}_2)}{\gamma_1} \frac{\sin(\nu \Delta y_1)}{\nu} e^{-\gamma_1(x_2 + y_2^{nm})} e^{i\nu(x_1 - y_1^{nm})} d\nu \tag{2.37}$$

$$C_2^{nm}(\mathbf{x}) = \frac{2}{\pi}\int_{C_R} \frac{1}{\gamma_1+\gamma_2}\frac{\sinh(\gamma_1\Delta y_2)}{\gamma_1}\frac{\sin(\nu\Delta y_1)}{\nu}e^{-\gamma_1 y_2^{nm}}e^{\gamma_2 x_2}e^{i\nu(x_1-y_1^{nm})}d\nu \quad (2.38)$$

$$C_3^{nm}(\mathbf{x}) = \frac{2}{\pi}\int_{C_R} \frac{1}{\gamma_1+\gamma_2}\frac{\sinh(\gamma_2\Delta y_2)}{\gamma_2}\frac{\sin(\nu\Delta y_1)}{\nu}e^{\gamma_2 y_2^{nm}}e^{-\gamma_1 x_2}e^{i\nu(x_1-y_1^{nm})}d\nu \quad (2.39)$$

$$C_4^{nm}(\mathbf{x}) = \frac{2}{\pi}\int_{C_R} \frac{1}{2\gamma_2}\frac{\gamma_2-\gamma_1}{\gamma_1+\gamma_2}\frac{\sinh(\gamma_2\Delta y_2)}{\gamma_2}\frac{\sin(\nu\Delta y_1)}{\nu}e^{\gamma_2(x_2+y_2^{nm})}e^{i\nu(x_1-y_1^{nm})}d\nu \quad (2.40)$$

$$C_5^{nm}(\mathbf{x}) = \begin{cases} \frac{i}{2k_2^2}[\pi k_2 a H_1^{(1)}(k_2 a)+2i], & n=m \\ \\ \frac{i\pi a}{2k_2}J_1(k_2 a)H_0^{(1)}(k_2|\mathbf{x}-\mathbf{y}^{nm}|) & ,n\neq m \end{cases} \quad (2.41)$$

In (2.36) and (2.41) "a" denotes the radii of the circular cell whose area is equivalent to the rectangular cell $2\Delta y_1 \times 2\Delta y_2$ [51].

Substituting (2.33) into (2.29) and writing the resulting expression for $\mathbf{x} = \mathbf{y}^{pq}$, $p = 1, 2, ..., 2N$, $q = 1, 2, ..., M_n$ one gets a linear system of equations for the field values of $u_s(\mathbf{y}^{pq})$. Note that in such a case the operator A is reduced to a square matrix with dimensions $(M_1 + M_2 + .. + M_{2N}) \times (M_1 + M_2 + .. + M_{2N})$ and the number of unknowns in the linear system is $(M_1 + M_2 + .. + M_{2N})$.

2.5 Near and Far Field Expressions of Scattered Wave

Since the field $u_s(\mathbf{x})$, consequently the total field $u(\mathbf{x})$, is now known at inner points of each cell S_{nm}, one can calculate the scattered field at any point $\mathbf{x} \in I\!R^2$ through the relation

$$u_s(\mathbf{x}) = \sum_{n=1}^{N}[k_1^2 \upsilon_1 \sum_{m=1}^{M_{2n-1}} u(\mathbf{y}^{nm})C^{nm}(\mathbf{x}) + k_2^2 \upsilon_2 \sum_{n=1}^{M_{2n}} u(\mathbf{y}^{nm})C^{nm}(\mathbf{x})]. \quad (2.42)$$

On the other hand the scattered far field at large distances from the surface in the upper half-space is described through the far field scattering amplitude $A(\hat{\mathbf{x}})$ defined by the asymptotic behavior

$$u_s(\mathbf{x}) = \frac{e^{ik_1|\mathbf{x}|}}{\sqrt{|\mathbf{x}|}}(A(\hat{\mathbf{x}}) + O(\frac{1}{|\mathbf{x}|})), \quad |\mathbf{x}| \to \infty, \quad x_2 > 0 \tag{2.43}$$

in the observation direction $\hat{\mathbf{x}} = \frac{\mathbf{x}}{|\mathbf{x}|} = (\cos\phi, \sin\phi)$, $\phi \in (0, \pi)$. This can be done by using the asymptotic behavior of $G_0(\mathbf{x}; \mathbf{y})$ for $|\mathbf{x}| \to \infty$, $x_2 > 0$, i.e.: $G_{0T}^{(2)}(\mathbf{x}; \mathbf{y})$ and $H_0^{(1)}(k_1|\mathbf{x} - \mathbf{y}|) + G_{0R}^{(1)}(\mathbf{x}; \mathbf{y})$. We first consider $G_{0T}^{(2)}(\mathbf{x}; \mathbf{y})$ given in (2.24) and make the following substitutions

$$x_1 = |\mathbf{x}|\cos\phi, \quad x_2 = |\mathbf{x}|\sin\phi, \quad \phi \in (0, \pi) \tag{2.44}$$

$$\nu = k_2\cos\alpha, \quad \gamma_2 = -ik_2\sin\alpha, \quad \alpha \in C^* \tag{2.45}$$

where C^* is the line illustrated in Figure 2.5. After some simple straightforward computations we get

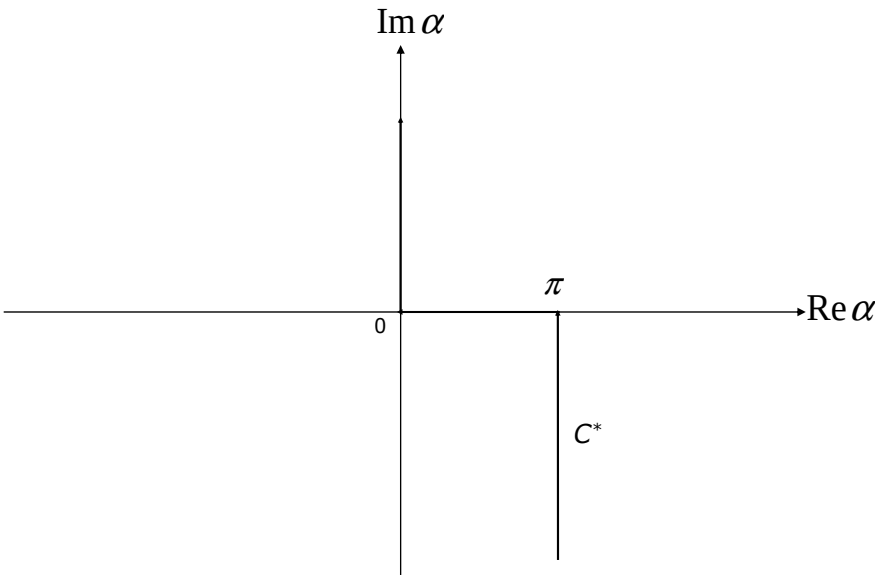


Figure 2.5: Mapping of C_R in the complex α-plane.

$$G_{0T}^{(2)}(|\mathbf{x}|, \phi; \mathbf{y}) = \frac{-ik_2}{2\pi}\int_{C^*} \xi(\alpha)e^{|\mathbf{x}|\eta(\alpha)}d\alpha \tag{2.46}$$

where

$$\eta(\alpha) = i(\sqrt{k_1^2 - k_2^2 \cos^2 \alpha}\sin\phi + k_2 \cos\alpha \cos\phi) \tag{2.47}$$

$$\xi(\alpha) = \frac{\sin\alpha}{\sqrt{k_1^2 - k_2^2\cos^2\alpha} + k_2 \sin\alpha} e^{-ik_2(y_1\cos\alpha + y_2 \sin\alpha)}. \tag{2.48}$$

The integral in (2.46) is now in the standard form susceptible to be evaluated for large values of $|\mathbf{x}|$ asymptotically by the classical saddle-point technique [49]. Indeed the saddle-point occurs at

$$\cos\alpha_s = \frac{k_1}{k_2}\cos\phi \qquad \mathrm{Re}\alpha_s \in (0, \pi). \tag{2.49}$$

Then following the known procedure for the saddle-point technique we obtain

$$\lim_{|\mathbf{x}|\to\infty} G_{0T}^{(2)}(|\mathbf{x}|, \phi; \mathbf{y}) \simeq \frac{e^{ik_1|\mathbf{x}|}}{|\mathbf{x}|}\frac{e^{i\frac{\pi}{4}}}{\sqrt{2\pi k_1}} T_1(\phi) e^{-i(k_1 y_1 \cos\phi + y_2\sqrt{k_2^2 - k_1^2\cos^2\phi})} + O(\frac{1}{|\mathbf{x}|^{3/2}}) \tag{2.50}$$

with

$$T_1(\phi) = \frac{2k_1\sin\phi}{k_1\sin\phi + \sqrt{k_2^2 - k_1^2\cos^2\phi}}. \tag{2.51}$$

By using the same procedure for $G_{0R}^{(1)}$ and using the asymptotic expression of $H_0^{(1)}$ one can obtain the asymptotic behavior of $H_0^{(1)}(k_1|\mathbf{x}-\mathbf{y}|) + G_{0R}^{(1)}(\mathbf{x};\mathbf{y})$ as follows:

$$\lim_{|\mathbf{x}|\to\infty}[H_0^{(1)}(k_1|\mathbf{x}-\mathbf{y}|) + G_{0R}^{(1)}(\mathbf{x};\mathbf{y})] \simeq \frac{e^{ik_1|\mathbf{x}|}}{|\mathbf{x}|}\frac{e^{i\frac{\pi}{4}}}{\sqrt{2\pi k_1}}[e^{-ik_1 y_1\cos\phi + y_2\sin\phi)}$$

$$+ R_1(\phi)e^{-ik_1(y_1\cos\phi - y_2\sin\phi)}] + O(\frac{1}{|\mathbf{x}|^{3/2}} \tag{2.52}$$

where

$$R_1(\phi) = \frac{k_1\sin\phi - \sqrt{k_2^2 - k_1^2\cos^2\phi}}{k_1\sin\phi + \sqrt{k_2^2 - k_1^2\cos^2\phi}}. \tag{2.53}$$

Then by using (2.42), (2.50) and (2.52) one can easily set the far field scattering amplitude $A(\hat{\mathbf{x}})$ as

$$A(\hat{\mathbf{x}}) = \frac{e^{i\pi/4}}{2\sqrt{2\pi k_1}} \sum_{n=1}^{N} [k_1^2 \upsilon_1 \sum_{m=1}^{M_{2n-1}} u(\mathbf{y}^{nm}) f_{nm}(\phi) + k_2^2 \upsilon_2 \sum_{m=1}^{M_{2n}} u(\mathbf{y}^{nm}) g_{nm}(\phi)] \quad (2.54)$$

where

$$f_{nm}(\phi) = \int_{S_{nm}} [e^{-ik_1(y_1 \cos\phi + y_2 \sin\phi)} + R_1(\phi) e^{-ik_1(y_1 \cos\phi - y_2 \sin\phi)}] d\mathbf{y}, \; y_2 > 0 \quad (2.55)$$

$$g_{nm}(\phi) = \int_{S_{nm}} T_1(\phi) e^{-i(k_1 y_1 \cos\phi + y_2 \sqrt{k_2^2 - k_1^2 \cos^2\phi})} d\mathbf{y}, \quad y_2 < 0. \quad (2.56)$$

The scattering cross-section per unit length, i.e., the echo width, defined as

$$\sigma_{2D}(\hat{\mathbf{x}}) := 2\pi \lim_{|\mathbf{x}| \to \infty} |\mathbf{x}| \, \frac{|u^s(\mathbf{x})|^2}{|u^i(\mathbf{x})|^2} \, , \quad (2.57)$$

that is,

$$\sigma_{2D}(\hat{\mathbf{x}}) := 2\pi |A(\hat{\mathbf{x}})|^2$$

is of particular interest in the scattering problems.

3 SCATTERING OF ELECTROMAGNETIC WAVES BY BODIES BURIED IN A HALF-SPACE WITH ROUGH SURFACE

In the previous section we presented an efficient and accurate method for the solution of scattering problems related to rough interfaces between two dielectric lossy half-spaces. Such a method can also be extended to solve the electromagnetic scattering problems from object in a layered media with rough interface. In the following a new method, which is based on the *buried object approach*, is presented.

3.1 Formulation of the Scattering Problem

Consider the two-dimensional scattering problem illustrated in Figure 3.1. In this configuration the space is separated into two-half spaces by a rough interface Γ which is same as described in Section 2.1. In the lower half-space $x_2 < f(x_1)$ an infinitely long cylindrical body D having a cross-section B with the Ox_1x_2 plane is located parallel to the Ox_3-axis. D can also be composed of several disjoint parts. The material of the body is inhomogeneous and its dielectric permittivity and conductivity are functions of location, namely, $\varepsilon = \varepsilon(\mathbf{x})$, $\sigma = \sigma(\mathbf{x})$ respectively, where $\mathbf{x} = (x_1, x_2)$ is the position vector in $\mathbb{R}^2$. The scattering problem considered here is to determine the effect of the body D as well as the roughness of the surface Γ on the propagation of electromagnetic waves excited in the upper half-space $x_2 > f(x_1)$. To this end the body is illuminated by a time-harmonic plane wave given in (2.1)

Because of the homogeneity of the problem in the Ox_3 direction and since we are considering cylindrical objects, the total electric field vector $\tilde{u}(\mathbf{x})$ will also be parallel to the Ox_3-axis i.e.: $\vec{E}(\mathbf{x}) = (0, 0, \tilde{u}(\mathbf{x}))$. Then the problem is reduced to a scalar one in terms of the total field function $\tilde{u}(\mathbf{x})$ which satisfies the reduced wave equation

$$\Delta\tilde{u} + \bar{k}^2(\mathbf{x})\tilde{u} = 0 \tag{3.1}$$

in the sense of distributions [48], where $\bar{k}(\mathbf{x})$ denotes the wave-number of the whole space.

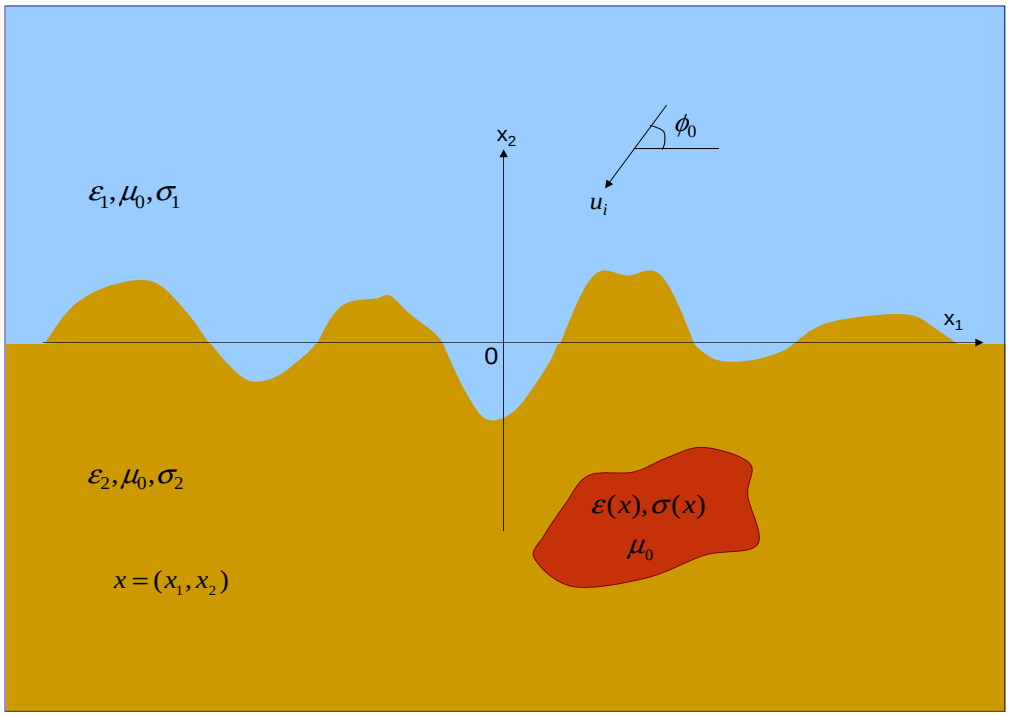


Figure 3.1: Geometry of the scattering problem related to buried object

Consider first the total field in the whole space for the same incident field (2.1) in the absence of body D. In such a case, the total field is nothing but the field due to the rough interface and its explicit expression $u(\mathbf{x}) = u_0(\mathbf{x}) + u_s(\mathbf{x})$ is derived in the previous section where $u_0(\mathbf{x})$ and $u_s(\mathbf{x})$ are given by (2.7) and (2.14). Then the contribution of the body D to the total field, i.e.: scattered field $\tilde{u}_s(\mathbf{x})$, consists in the difference $\tilde{u}_s(\mathbf{x}) = \tilde{u}(\mathbf{x}) - u(\mathbf{x})$, and satisfies

$$\Delta\tilde{u}_s + k^2(\mathbf{x})\tilde{u}_s = -k_2^2 v(\mathbf{x})\tilde{u} \tag{3.2}$$

under the Sommerfeld radiation condition. Here $v(\mathbf{x})$ stands for the *object function* related to body D, namely,

$$v(\mathbf{x}) = \frac{\varepsilon(\mathbf{x}) + i\frac{\sigma(\mathbf{x})}{\omega}}{\varepsilon'(\mathbf{x}) + i\frac{\sigma'(\mathbf{x})}{\omega}} - 1 \tag{3.3}$$

where

$$\varepsilon'(\mathbf{x}) = \begin{cases} \varepsilon_1, & x_2 > f(x_1) \\ \varepsilon_2, & x_2 < f(x_1) \end{cases} \tag{3.4}$$

and

$$\sigma'(\mathbf{x}) = \begin{cases} \sigma_1, & x_2 > f(x_1) \\ \sigma_2, & x_2 < f(x_1) \end{cases}. \tag{3.5}$$

From (3.3) one can easily conclude that the function $\upsilon(\mathbf{x})$ is identically zero outside the region B.

Let $\bar{G}(\mathbf{x};\mathbf{y})$ be the Green's function of the two-part space with rough interface Γ (see Figure 2.2). Then one can convert (3.2) into a Fredholm integral equation of second kind for the scattered field $\tilde{u}_s(\mathbf{x})$, namely,

$$\tilde{u}_s(\mathbf{x}) = k_2^2 \int_B \bar{G}(\mathbf{x};\mathbf{y})\upsilon(\mathbf{y})(u(\mathbf{y}) + \tilde{u}_s(\mathbf{y}))d\mathbf{y}. \tag{3.6}$$

When $\bar{G}(\mathbf{x};\mathbf{y})$ is known, (3.6) can be solved through a method based on MoM [27, 50, 51]. Note that in [27] such a method is applied for the bodies buried in a half-space with planar boundary.

Assume now that $\bar{G}(\mathbf{x};\mathbf{y})$ and $u(\mathbf{y})$ are given. Then one can solve $\tilde{u}(\mathbf{x})$ at inner points of the object by first dividing the region B into P cells $S_p,\ p = 1, 2, .., P$. This yields

$$\tilde{u}(\mathbf{x}) = u(\mathbf{x}) + k_2^2 \sum_{p=1}^{P} \int_{S_p} \bar{G}(\mathbf{x};\mathbf{y})\upsilon(\mathbf{y})\tilde{u}(\mathbf{y})d\mathbf{y}. \tag{3.7}$$

When the sizes of the cells are chosen sufficiently small such that both $\tilde{u}$ and υ may be assumed to be constant over a given cell, (3.7) can be converted into a system of linear equations of the form

$$(I - Q)\tilde{u} = u \tag{3.8}$$

where I is the unit matrix while Q is a $P \times P$ square matrix with elements

$$Q_{qp} = k_2^2 \upsilon_p \int_{S_p} \bar{G}(\mathbf{x}_q;\mathbf{y})d\mathbf{y}. \tag{3.9}$$

In (3.8) $\tilde{u}$ and u are vectors with elements $\tilde{u}_p = \tilde{u}(\mathbf{x}_p)$ and $u_p = u(\mathbf{x}_p)$, $p = 1, 2, .., P$, respectively, where $\mathbf{x}_p$ denotes the center point of the p'th cell, while υ_p in (3.9) is the value of the object function at the same point.

Then by taking the discrete form of (3.6) into account one can write the scattered field at any point in the space as

$$\tilde{u}_s(\mathbf{x}) = k_2^2 \sum_{p=1}^{P} \upsilon_p \tilde{u}_p \int_{S_p} \bar{G}(\mathbf{x}; \mathbf{y}) d\mathbf{y}. \tag{3.10}$$

The integral of $\bar{G}(\mathbf{x}; \mathbf{y})$ appearing in (3.9) and (3.10) can be calculated by using one of the numerical integral techniques. Notice that (3.10) can also be used to calculate asymptotic expression of the scattered field for $|\mathbf{x}| \to \infty$ through the asymptotic behavior of $\bar{G}(\mathbf{x}; \mathbf{y})$ which will be given in the Section 3.3. Before going more further it will be convenient to give an expression of the Green's function $\bar{G}(\mathbf{x}; \mathbf{y})$.

3.2 Green's Function of Two Half-Space Medium with Rough Interface

By definition the Green's function $\bar{G}(\mathbf{x}; \mathbf{y})$ of the two-half spaces medium with rough interface Γ is the solution of the problem

$$\Delta \bar{G}(\mathbf{x}; \mathbf{y}) + k^2(\mathbf{x}) \bar{G}(\mathbf{x}; \mathbf{y}) = -\delta(\mathbf{x} - \mathbf{y}) \tag{3.11}$$

$$\bar{G} \ \textit{and} \ \frac{\partial \bar{G}}{\partial n} \ \textit{are continuous on} \ \Gamma \tag{3.12}$$

with the appropriate radiation condition as $|\mathbf{x}| \to \infty$. It is obvious that $\bar{G}(\mathbf{x}; \mathbf{y})$ is nothing but the total field at the point $\mathbf{x} \in I\!R^2$ due to a line source with normalized strength $\frac{1}{i\omega\mu_0}$ located at $\mathbf{y} \in I\!R^2$. In other words, to obtain $\bar{G}$ one has to solve the scattering problem related to the rough surface Γ for the case of line source illumination, which is treated here in the following way:

By using the *buried object approach*, which is presented in Section 2.2, the scattering problem described above is reduced to the solution of scattering of cylindrical electromagnetic waves from 2N buried homogeneous objects in a two-part space having a planar interface (see Figure 2.2).

In order to formulate the problem more easily consider now the Green's function $G_0(\mathbf{x};\mathbf{y})$ of two-half spaces medium separated by the plane $x_2 = 0$ whose explicit expression is given in Section 2.3. Hence, the contribution of the regions $D_1, D_2, ..., D_{2N}$ to $\bar{G}(\mathbf{x};\mathbf{y})$, say $G_s(\mathbf{x};\mathbf{y})$, consists in the difference

$$G_s(\mathbf{x};\mathbf{y}) = \bar{G}(\mathbf{x};\mathbf{y}) - G_0(\mathbf{x};\mathbf{y}) \tag{3.13}$$

and satisfies the reduced wave equation

$$\triangle G_s(\mathbf{x};\mathbf{y}) + k^2(x_2)G_s(\mathbf{x};\mathbf{y}) = -k^2(x_2)\upsilon_R(\mathbf{x})\bar{G}(\mathbf{x};\mathbf{y}) \tag{3.14}$$

in the sense of distribution under the radiation condition for $|\mathbf{x}| \to \infty$. Here, the function $\upsilon_R(\mathbf{x})$ is the object function related to the regions $D_1, D_2, ..., D_{2N}$ and is given by the relation (2.13).

The Green's function $G_0(\mathbf{x};\mathbf{y})$ of the two-part space with planar interface permits us to convert the differential equation (3.14) into the following Fredholm integral equation of the second kind:

$$\begin{aligned} G_s(\mathbf{x};\mathbf{y}) = k_1^2\upsilon_1 \sum_{n=1}^{N} \int_{B_{2n-1}} G_0(\mathbf{x};\mathbf{z})(G_0(\mathbf{z};\mathbf{y}) + G_s(\mathbf{z};\mathbf{y}))d\mathbf{z} \\ +k_2^2\upsilon_2 \sum_{n=1}^{N} \int_{B_{2n}} G_0(\mathbf{x};\mathbf{z})(G_0(\mathbf{z};\mathbf{y}) + G_s(\mathbf{z};\mathbf{y}))d\mathbf{z}. \end{aligned} \tag{3.15}$$

In the sequel we will describe a method which is an application of MoM to solve $G_s(\mathbf{x};\mathbf{y})$ from (3.15) [50, 51]. To this aim we first write (3.15) in an abbreviated form

$$(I - K)G_s(\mathbf{x};\mathbf{y}) = g(\mathbf{x};\mathbf{y}), \quad \mathbf{x},\mathbf{y} \in I\!R^2 \tag{3.16}$$

where K is the linear operator defined by

$$KG_s(\mathbf{x};\mathbf{y}) = \sum_{n=1}^{N}[k_1^2\upsilon_1 \int_{B_{2n-1}} G_0(\mathbf{x};\mathbf{z})G_s(\mathbf{z};\mathbf{y})d\mathbf{z} + k_2^2\upsilon_2 \int_{B_{2n}} G_0(\mathbf{x};\mathbf{z})G_s(\mathbf{z};\mathbf{y})d\mathbf{z}] \tag{3.17}$$

while $g(\mathbf{x};\mathbf{y})$ is the known function

$$g(\mathbf{x};\mathbf{y}) = \sum_{n=1}^{N}[k_1^2\upsilon_1 \int_{B_{2n-1}} G_0(\mathbf{x};\mathbf{z})G_0(\mathbf{z};\mathbf{y})d\mathbf{z} + k_2^2\upsilon_2 \int_{B_{2n}} G_0(\mathbf{x};\mathbf{z})G_0(\mathbf{z};\mathbf{y})d\mathbf{z}]. \tag{3.18}$$

Consider now the n'th region B_n and divide it into M_n small cells which allows one to write

$$\int_{B_n} G_0(\mathbf{x};\mathbf{z})G_s(\mathbf{z};\mathbf{y})d\mathbf{z} = \sum_{m=1}^{M_n} \int_{S_{nm}} G_0(\mathbf{x};\mathbf{z})G_s(\mathbf{z};\mathbf{y})d\mathbf{z} \tag{3.19}$$

where S_{nm} denotes m'th cell of the region B_n. If S_{nm} is small enough one can make the approximation $G_s(\mathbf{z};\mathbf{y}) \simeq G_s(\mathbf{z}^{nm};\mathbf{y})$ for the scattered field inside the related cell, where $\mathbf{z}^{nm} = (z_1^{nm}, z_2^{nm})$ stands for the center point of the cell S_{nm}. Then one has

$$\int_{B_n} G_0(\mathbf{x};\mathbf{z})G_s(\mathbf{z};\mathbf{y})d\mathbf{z} \simeq \sum_{m=1}^{M_n} G_s(\mathbf{z}^{nm};\mathbf{y})C^{nm}(\mathbf{x}) \tag{3.20}$$

where $C^{nm}(\mathbf{x})$ is given by (2.34).

Following the same analysis to solve (3.15), (3.16) can be reduced to a linear system of equations for the field values of $G_s(\mathbf{z}^{pq};\mathbf{y})$. Note that in such a case the operator K is reduced to a square matrix with dimensions $(M_1 + M_2 + .. + M_{2N}) \times (M_1 + M_2 + .. + M_{2N})$ and the number of unknowns in the linear system is $(M_1 + M_2 + .. + M_{2N})$.

Since the field $G_s(\mathbf{z};\mathbf{y})$, consequently the Green's function $\bar{G}(\mathbf{z};\mathbf{y})$, is now known at inner points of each cell S_{nm}, one can calculate $G_s(\mathbf{x};\mathbf{y})$ for any $\mathbf{x},\mathbf{y} \in I\!R^2$ through the relation

$$G_s(\mathbf{x};\mathbf{y}) = \sum_{n=1}^{N}[k_1^2 v_1 \sum_{m=1}^{M_{2n-1}} \bar{G}(\mathbf{z}^{nm};\mathbf{y})C^{nm}(\mathbf{x}) + k_2^2 v_2 \sum_{n=1}^{M_{2n}} \bar{G}(\mathbf{z}^{nm};\mathbf{y})C^{nm}(\mathbf{x})] \tag{3.21}$$

which yields $\bar{G}(\mathbf{x};\mathbf{y})$ for any $x, y \in R^2$ by taking (3.13) into consideration.

3.3 Far Field Expression of the Scattered Wave

Through the asymptotic behavior of $\bar{G}(\mathbf{x};\mathbf{y})$ and (3.6) one can calculate the far field scattering amplitude of the scattered field $\tilde{u}_s(x)$. On the other hand the far field behavior of the Green's function $\bar{G}(\mathbf{x};\mathbf{y})$ for $|\mathbf{x}| \to \infty$ in the region $x_2 > 0$ is described through the far field scattering amplitude $A_\phi(\hat{\mathbf{x}};\mathbf{y})$ defined by the asymptotic behavior

$$\bar{G}(\mathbf{x};\mathbf{y}) = \frac{e^{ik_1|\mathbf{x}|}}{\sqrt{|\mathbf{x}|}}(A_\phi(\hat{\mathbf{x}};\mathbf{y}) + O(\frac{1}{|\mathbf{x}|})), \quad |\mathbf{x}| \to \infty, \quad x_2 > 0 \tag{3.22}$$

in the observation direction $\hat{\mathbf{x}} = \frac{\mathbf{x}}{|\mathbf{x}|} = (\cos\phi, \sin\phi),\ \phi \in (0,\pi)$. This requires to have the asymptotic expressions of both $G_0(\mathbf{x};\mathbf{y})$ which given in Section 2.5 and $G_s(\mathbf{x};\mathbf{y})$ for $|\mathbf{x}| \to \infty,\ x_2 > 0$. The asymptotic behavior of $G_s(\mathbf{x};\mathbf{y})$ can be obtained from (3.21) by using (2.50) and (2.52). Then one has

$$\begin{aligned} A_\phi(\hat{\mathbf{x}};\mathbf{y}) = \frac{e^{i\pi/4}}{2\sqrt{2\pi k_1}} \sum_{n=1}^{N} [k_1^2 \upsilon_1 \sum_{m=1}^{M_{2n-1}} \bar{G}(\mathbf{z}^{nm};\mathbf{y})\Psi_{nm}(\phi) \\ + k_2^2 \upsilon_2 \sum_{m=1}^{M_{2n}} \bar{G}(\mathbf{z}^{nm};\mathbf{y})\Theta_{nm}(\phi)] \\ + \frac{e^{i\frac{\pi}{4}}}{\sqrt{2\pi k_1}} T_1(\phi) e^{-i(k_1 y_1 \cos\phi + y_2\sqrt{k_2^2 - k_1^2\cos^2\phi})} \end{aligned} \tag{3.23}$$

where

$$\Psi_{nm}(\phi) = \int_{S_{nm}} [e^{-i(k_1 z_1 \cos\phi + z_2 \sin\phi)} + R_1(\phi) e^{-ik_1(z_1\cos\phi - z_2\sin\phi)}] d\mathbf{z},\ z_2 > 0 \tag{3.24}$$

$$\Theta_{nm}(\phi) = \int_{S_{nm}} T_1(\phi) e^{-ik_1(z_1\cos\phi + z_2\sqrt{k_2^2 - k_1^2\cos^2\phi})} d\mathbf{z}, \quad z_2 < 0. \tag{3.25}$$

One can now write the far field scattering amplitude $\tilde{u_s}(\mathbf{x})$, say $\tilde{A}(\phi)$ through (3.6) and (3.23), namely

$$\tilde{A}(\phi) = k_2^2 \sum_{p=1}^{P} \upsilon_p \tilde{u}_p \int_{S_p} A_\phi(\hat{\mathbf{x}};\mathbf{y}) d\mathbf{y} \tag{3.26}$$

4 NUMERICAL IMPLEMENTATION

In this section we give some numerical results which demonstrate the accuracy, effectiveness and validation limits of the proposed method for both cases. Along this line the effects of some parameters such as rms height and correlation length of the surface, incidence direction, electromagnetic properties of the lower half-space as well as physical and geometrical properties of the objects are examined. The spectral integrals appearing in the right hand side of (2.22) to (2.25) and (2.36) to (2.41) are calculated through the FFT algorithm. It is worth to note that although these functions have a quite cumbersome appearance, their samples can be still calculated in a fast and efficient way by means of FFT codes. The accuracy of the FFT calculations was also shown by evaluating the integrals in (2.22) to (2.25) and (2.36) to (2.41) through the conventional numerical integration methods. In all examples the upper half-space is assumed to be air.

4.1 Numerical Results for Scattering from Rough Surface

We first present the results which are obtained through the method given in Section 2 for the scattering from rough surfaces.

The first two examples are devoted to the validation of the proposed method. To this aim we first consider a surface having a trigonometric variation $x_2 = -0.02\lambda cos(2\pi x_1)$ in the interval $x_1 \in (-20\lambda, 20\lambda)$, i.e.: roughness length is $L = 40\lambda$, where λ is the free-space wavelength. We compare the results of both analytical solution given in [52] and of the proposed method here, for the case of $\phi_0 = \pi/3$. In the evaluation of the method the sizes of the cells are chosen as $\frac{\lambda}{15} \times \frac{\lambda}{150}$. The lower half-space is assumed to be dry soil with parameters $\varepsilon_2 = 3.6\varepsilon_0$ and $\sigma_2 = 10^{-5}(S/m)$. Figure 4.1 shows the variations of the amplitudes of the scattered field on a certain line $x_2 = 2\lambda$ in the upper half-space with respect to x_1 obtained through both methods. Both method's results are agree with each other.

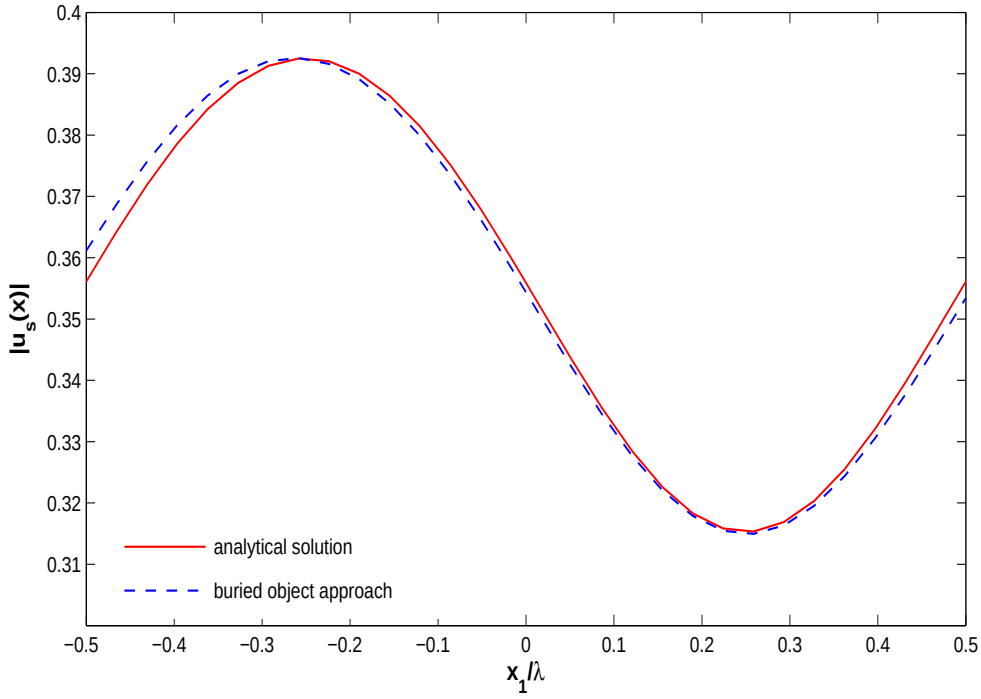


Figure 4.1: Variation of $|u_s|$ versus x_1/λ on the plane $x_2 = 2\lambda$ for a sinusoidal rough surface.

In Figure 4.2 the average coherent scattering cross-sections of the present method is compared with the small-perturbation method for a random surface with rms

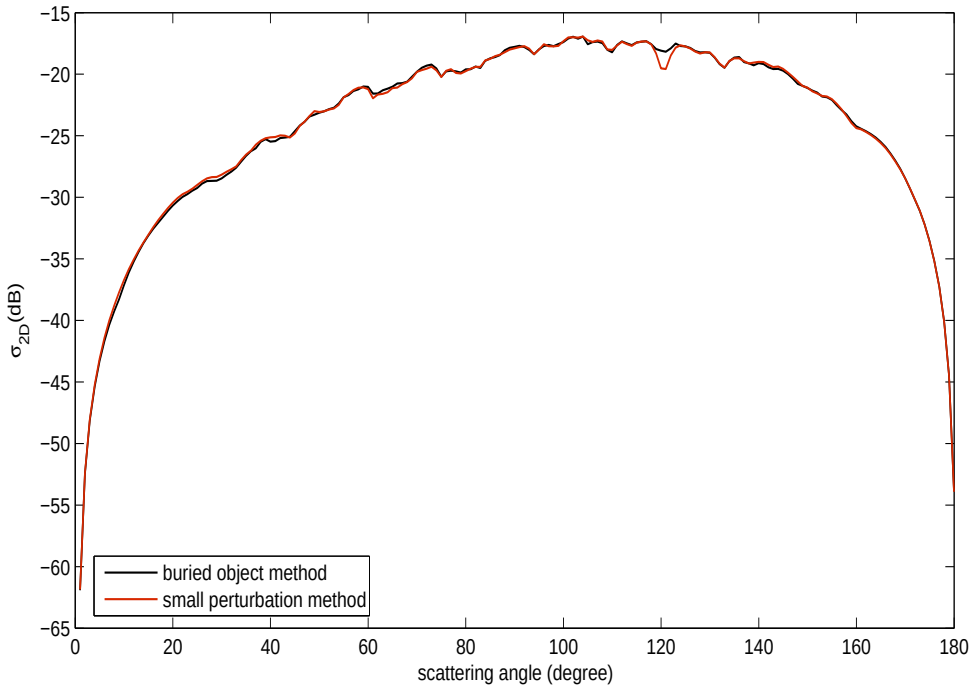


Figure 4.2: Comparison of the average cohorent scattering cross-sections of the buried object approach and the small perturbation method after 150 realizations

height 0.01λ, correlation length 0.3λ and $L = 8\lambda$ over dry soil. The averages are calculated after 150 realizations and the incidence direction is $\phi_0 = \pi/3$. As can be observed from the figures the results of the present method match with those of the existing methods in the near and far field region.

In Figure 4.3 the scattering widths corresponding different Gaussian correlated random surfaces having rms heights and correlation lengths $\sigma_r = 0.05\lambda, \ell_c = 0.15\lambda$; $\sigma_r = 0.5\lambda, \ell_c = 0.15\lambda$ and $\sigma_r = 0.5\lambda, \ell_c = 0.5\lambda$, respectively, are demon-

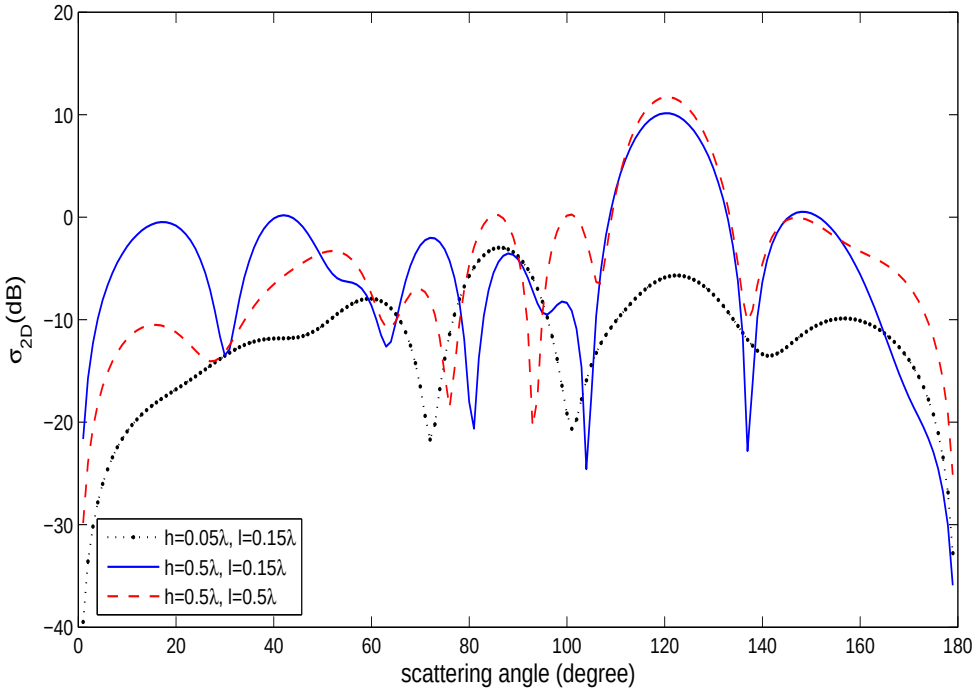


Figure 4.3: SW(σ_{2D}) versus observation angle ϕ for the surfaces having different rms heights and correlation lengths.

strated. The incidence direction is $\phi_0 = \pi/3$. Obviously, these parameters have a strong effect on scattered wave in the far field region.

As a subsequent example we consider a smoothly varying surface having function

$$f(x_1) = \begin{cases} 0.72x_1 \cos(0.5\pi x_1) e^{\frac{x_1}{3}}(1 + 0.2x_1), & x_1 \in (-5\lambda, 0); \\ 0.66x_1 \cos(0.5\pi x_1) e^{\frac{-8x_1}{15}}, & x_1 \in (0, 5\lambda); \\ 0, & \text{otherwise.} \end{cases}$$

with roughness length $L = 10\lambda$ separating air and dry soil. The surface is represented by 6 regions whose three of them are located in the air. These regions

are divided into square cells with dimensions $\frac{\lambda}{10} \times \frac{\lambda}{10}$. Then total number of cells created is 190 which yields a linear system of equations with 190 unknowns. Figure 4.4 shows the variation of the amplitude of the total electric field on a rectangular domain $12\lambda \times 6\lambda$ which contains the surface as well in the case of normal incidence $\phi_0 = \pi/2$. Note that such a surface is highly rough and creates regions comparable to the wavelength which means that we examine the scattering phenomena in the resonance region.

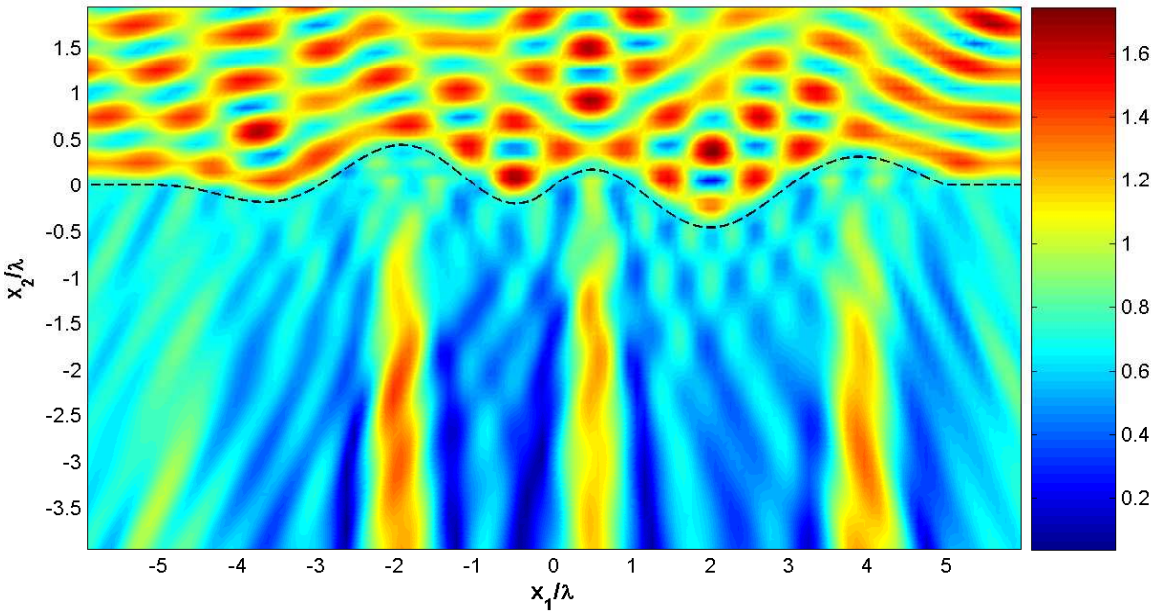


Figure 4.4: Variation of the amplitude of the total field for a smoothly varying air-dry soil interface.

Figure 4.5 illustrates the variation of the amplitude of the total field on the rectangular region with side lengths $6\lambda \times 5\lambda$ for a random surface with rms height $\sigma_r = 0.3\lambda$, correlation length $\ell_c = 0.2\lambda$ for a Gaussian distribution and $L = 4\lambda$ [47].

The results are given in the case of normal incidence to the air-dry soil interface with the same parameters in the previous example. Since the surface has a rapid variation the cell sizes are chosen as $\frac{\lambda}{32} \times \frac{\lambda}{20}$. In this case the total cell number is 690. By comparing both results given in Figure 4.4 and Figure 4.5 one can easily observe the strong effect of the roughness on propagation of electromagnetic field. Obviously, the contribution of the rapidly varying surface in Figure 4.5 to the total field is more stronger.

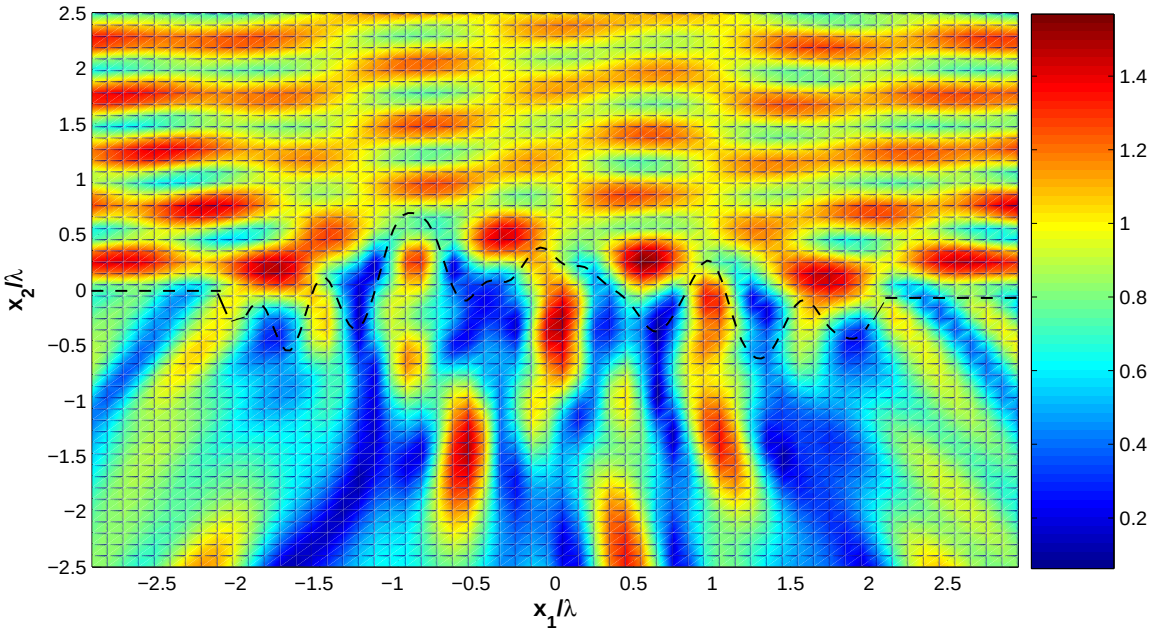


Figure 4.5: Variation of the amplitude of the total field for a random air-dry soil interface with $\sigma_r = 0.3\lambda, \ell_c = 0.2\lambda, L = 4\lambda$.

In order to see the effect of the material properties of the lower half-space we consider two different materials, namely dry and wet soil with electromagnetic parameters $\varepsilon_2 = 3.6\varepsilon_0$, $\sigma_2 = 10^{-5}(S/m)$ and $\varepsilon_2 = 30\varepsilon_0$, $\sigma_2 = 0.02(S/m)$, respectively. In both cases the surface is a random one with parameters $\sigma_r = 0.2\lambda$, $\ell_c = 0.2\lambda$ and $L = 4\lambda$. The number of cells is 646 with cell sizes $\frac{\lambda}{32} \times \frac{\lambda}{24}$ while the incidence direction is $\phi_0 = \pi/2$. The amplitudes of the total field on a rectangular region $6\lambda \times 3\lambda$ for the cases of dry and wet soil backgrounds are given in Figure 4.6 and Figure 4.7, respectively. Comparison of the results given in Figure 4.6 and Figure 4.7 clearly shows that the total field in the lower half-space for the medium with higher conductivity tends to zero, as expected, while the scattering effect is more strong in upper half-space.

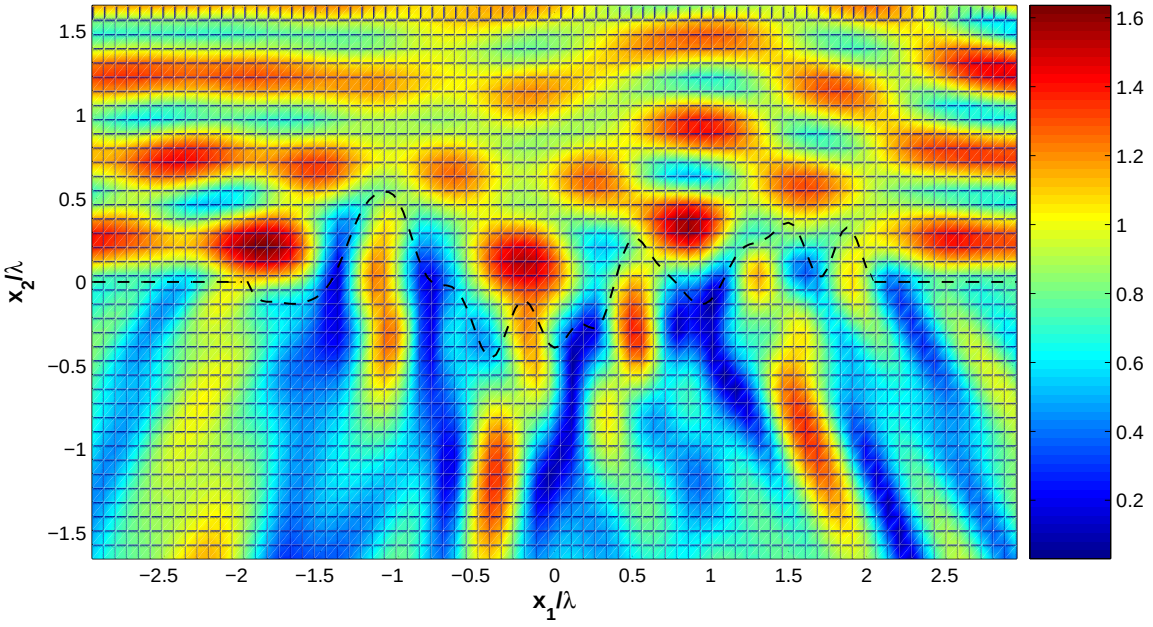


Figure 4.6: Variation of the amplitude of the total field for a random air-dry soil interface with $\sigma_r = 0.2\lambda, \ell_c = 0.2\lambda, L = 4\lambda$.

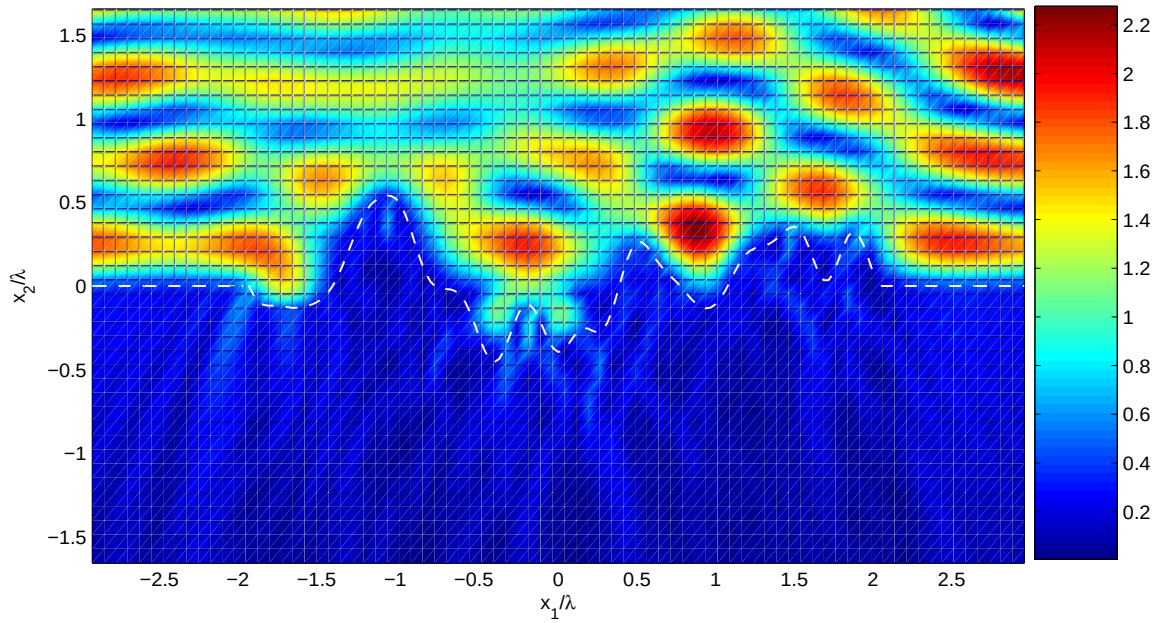


Figure 4.7: Variation of the amplitude of the total field for a random air-wet soil interface with $\sigma_r = 0.2\lambda, \ell_c = 0.2\lambda, L = 4\lambda$.

In Figure 4.8 and Figure 4.9 we present the variations of the amplitudes of the total field for two different incidence directions $\phi_0 = \pi/2$ and $\phi_0 = \pi/4$ for the case of random air-mica interface with parameters $\sigma_r = 0.2\lambda, \ell_c = 0.7\lambda$ and

$L = 6\lambda$. The chosen number of cells is 546 and sizes of cells are $\frac{\lambda}{21} \times \frac{\lambda}{28}$. Note that the electromagnetic parameters of mica are $\varepsilon = 5.4\varepsilon_0$ and $\sigma = 10^{-15}(S/m)$.

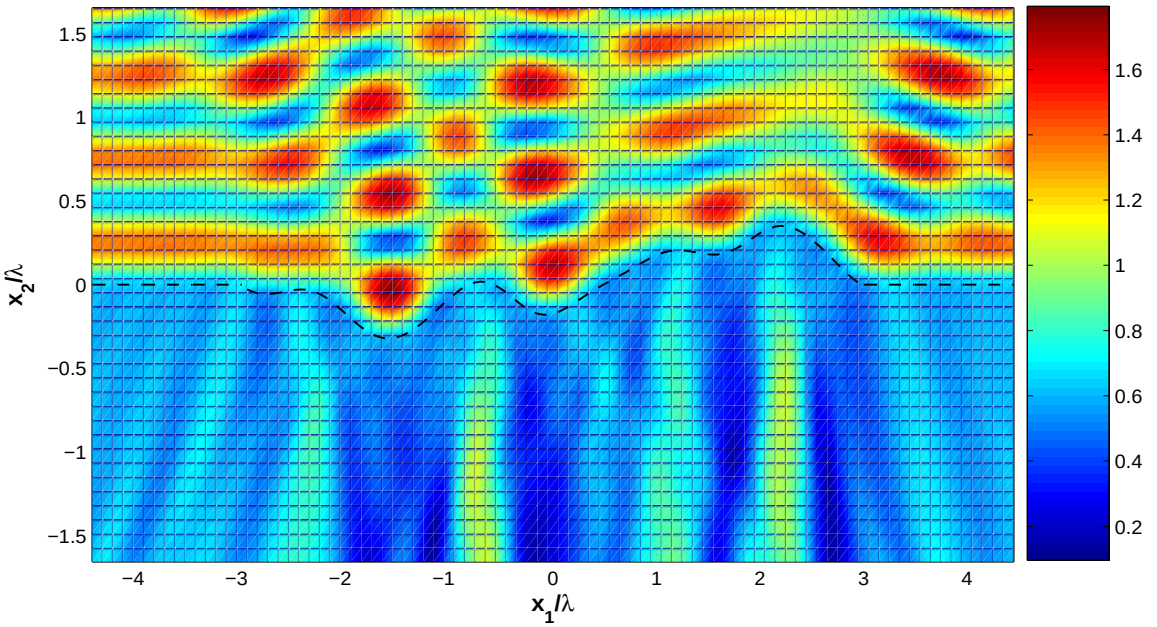


Figure 4.8: Variation of the amplitude of the total field for a random air-mica interface with $\sigma_r = 0.2\lambda, \ell_c = 0.6\lambda, L = 7\lambda$ and $\phi_0 = \pi/2$.

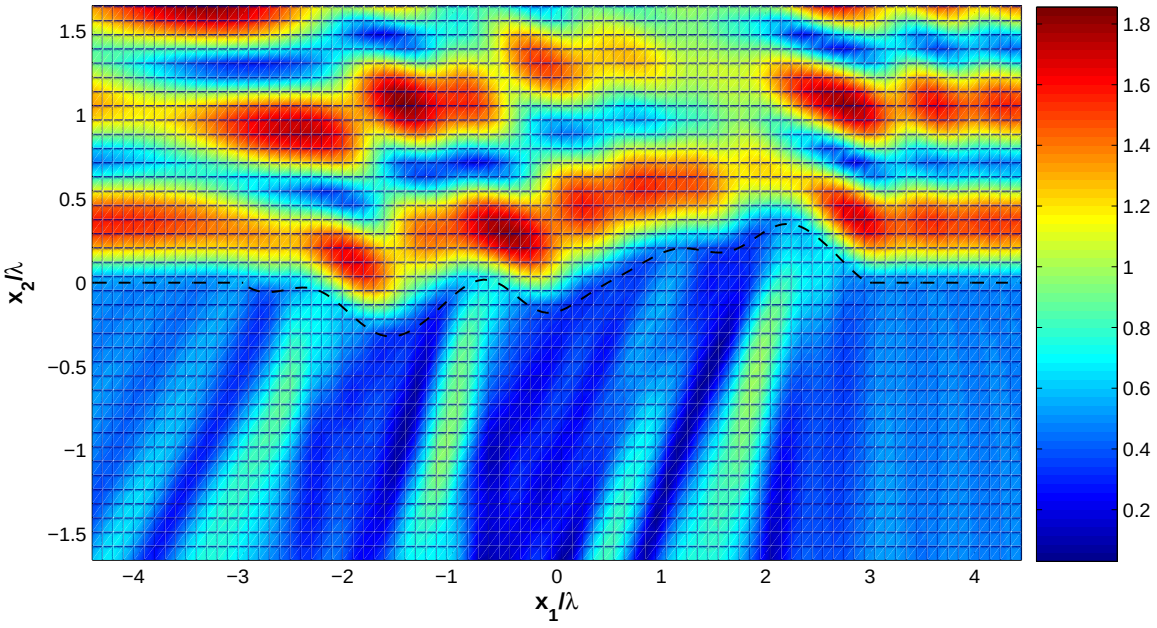


Figure 4.9: Variation of the amplitude of the total field for a random air-mica interface with $\sigma_r = 0.2\lambda, \ell_c = 0.6\lambda, L = 7\lambda$ and $\phi_0 = \pi/4$.

In the last example we consider a random surface with parameters $\sigma_r = 0.4\lambda$, $\ell_c = 0.5\lambda$ and $L = 10\lambda$ separating air and sea ($\varepsilon = 72\varepsilon_0$, $\sigma = 4(S/m)$). The variation of the total field on a certain domain is illustrated in Figure 4.10 for the incidence angle $\phi_0 = \pi/4$. As can easily be observed that the total field vanishes in the half-space $x_2 < 0$ although there are regions filled by air below the plane $x_2 = 0$. Whereas in those regions the field should not vanish. So the results are inaccurate. This is due to the fact that the field $u_0(x)$ vanishes in the region $x_2 < 0$

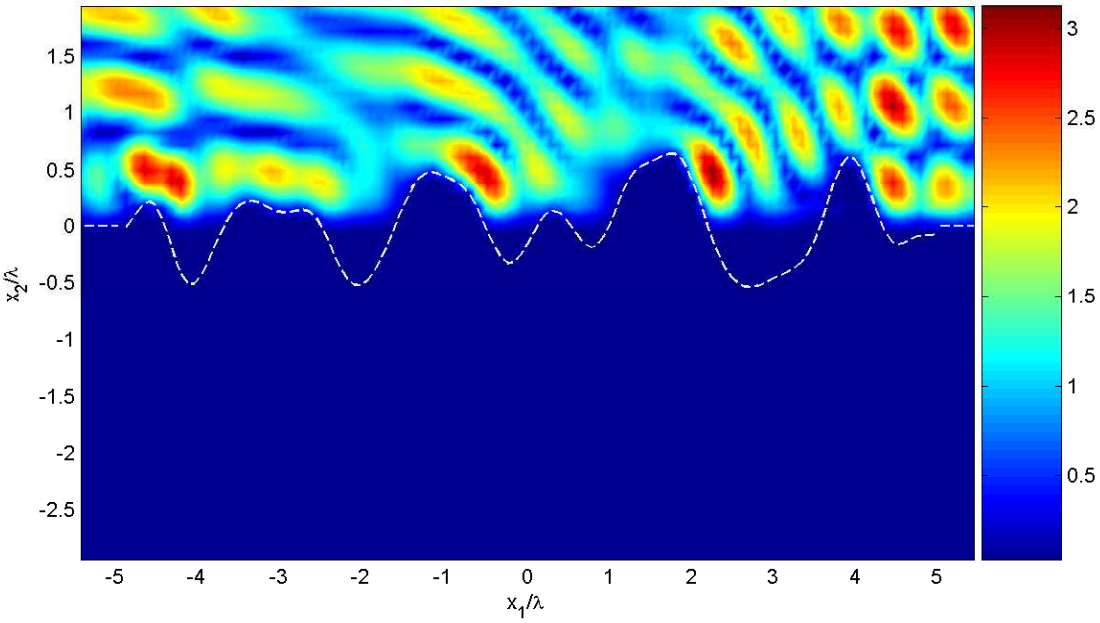


Figure 4.10: Variation of the amplitude of the total field for a random air-sea interface with $\sigma_r = 0.4\lambda, \ell_c = 0.5\lambda, L = 10\lambda$.

when the lower half-space is a highly conducting medium. Then one can easily conclude that the integrals over the regions $B_2, ...B_{2n}$ in the right hand-side of (2.31) tends to zero. This means that there is no interaction between the incident field and the bodies $D_2, ...D_{2n}$ which is actually not true. It has been observed that the method is not valid for highly conductive background medium having a conductivity $\sigma_2 > 10^{-2}(S/m)$.

In order to give an idea about the computational cost of the present method compared to the available surface based-integral methods we consider two surfaces of same rms height $\sigma_r = 0.3\lambda$, roughness length $L = 8.5\lambda$ and having different correlation lengths $\ell_c = 0.5\lambda$ and $\ell_c = 0.05\lambda$. For the surface with correlation length 0.5λ the number of unknowns in the present method is 615 for a chosen

cell size $\frac{\lambda}{15} \times \frac{\lambda}{15}$ while the surface based integral methods yield minimum 166 unknowns for a chosen line segment size $\frac{\lambda}{15}$. On the other hand when the surface has a correlation length 0.05λ, that is a rapidly varying one, the number of unknowns becomes 439 for *buried object approach* and 503 for surface integral methods for the same cell and segment sizes given above. From these examples and other numerical implementations we observe that the *buried object approach* is slower than surface integral approaches when the surface has a slowly varying profile. On the other hand for rapidly varying surface profiles the computational cost of the present method is comparable to those of the surface based integral methods. Although it is not within the scope of this study, the computational cost can be reduced by using fast algorithms such as fast multilevel techniques adopted to MoM [53].

It should be noted that for fine scale surfaces one has to divide the surface into very small regions which causes instabilities in the solution. Similar problems has been observed in the FDTD analysis of the rough surface scattering.

4.2 Numerical Results for Scattering from Objects Buried under a Rough Surface

Here some illustrative numerical results are given for the scattering of electromagnetic waves from bodies buried under a rough surface, which are obtained via the method given in Section 3.

The first example is devoted to the validation of the proposed method. To this end we consider a dielectric circular cylinder buried beneath a sinusoidal slightly rough surface. The parameters of this example are chosen as exactly the same with those given in [31]; i.e. $f(x) = 0.0064\lambda cos(\frac{2\pi}{0.4\lambda}x)$, $\varepsilon_1 = \varepsilon_0,\ \varepsilon_2 = 4\varepsilon_0, \sigma_2 = 2.22.10^{-5}(S/m), \varepsilon = 2.25\varepsilon_0$, where λ is the free space wavelength. The cylinder has a radii 0.16λ and its center is located at $(0, 1.3\lambda)$. It is illuminated by a plane wave with incidence direction $\phi_0 = \frac{\pi}{3}$ and frequency $f = 400MHz$. The scattering widths for the cases of the flat and sinusoidal interfaces are shown in Figure 4.11. The results of this example match completely those given in [31].

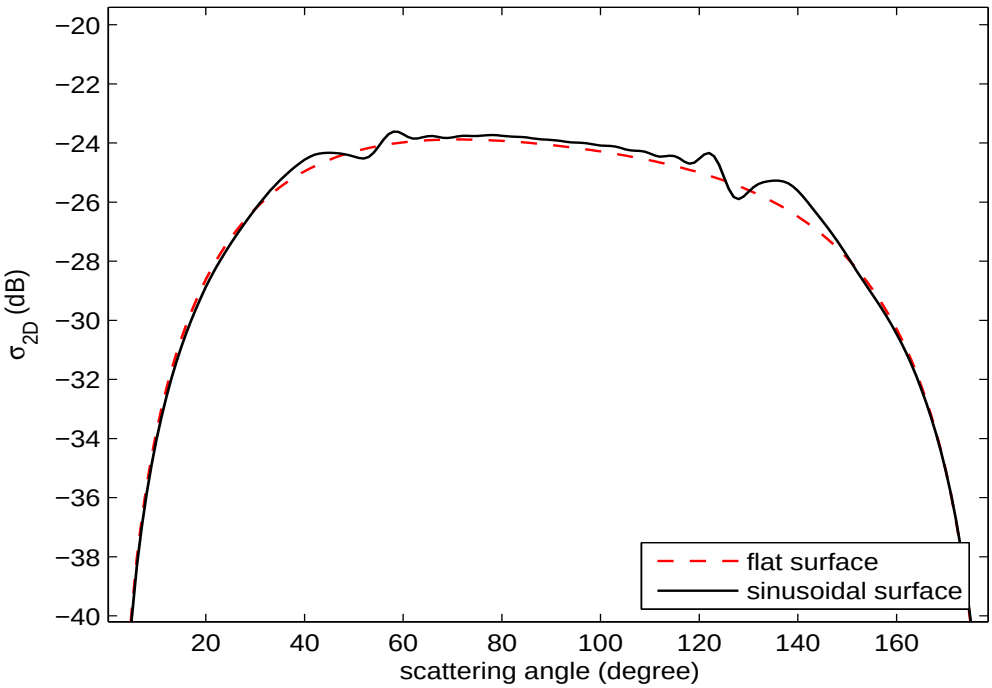


Figure 4.11: Comparison of the scattering widths due to a circular cylinder buried under a flat and sinusoidal rough interfaces.

Scattering widths corresponding for three cylinders having circular, rectangular and elliptical cross sections and buried in dry soil ($\varepsilon_2 = 3.6\varepsilon_0, \sigma_2 = 10^{-5}(S/m)$) under a Gaussian correlated random surface with rms height $\sigma_r = 0.4\lambda$, correlation length $\ell_c = 0.3\lambda$ and roughness length $L = 6\lambda$ are demonstrated in Figure 4.12. In the numerical implementation of the method both surface and the bodies are divided into rectangular cells with cell sizes $\frac{\lambda}{20} \times \frac{\lambda}{20}$. One can see the strong effects of the geometrical parameters of the objects on scattered wave in the far field region. In this example the bodies are illuminated by a normally incident wave.

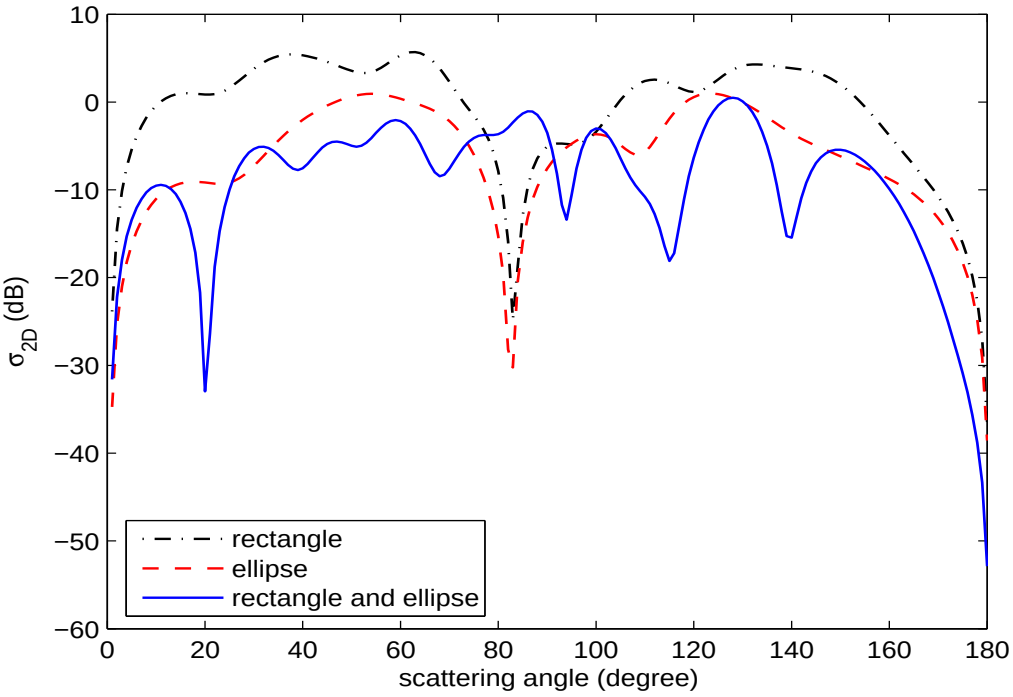


Figure 4.12: Scattering widths values corresponding three different object configurations buried under a random surface with $\sigma_r = 0.4\lambda, \ell_c = 0.3\lambda$ and $L = 6\lambda$.

In order to see the effect of the roughness level on the scattered field from buried bodies, we consider a circular cylinder buried the beneath a rough surface whose variation is given by $f(x_1) = he^{-\frac{x}{3}-\frac{|x|}{3}\frac{|x|}{5}}cos(\frac{3\pi x_1}{2\lambda})$ between $x_1 = -3\lambda$ and $x_1 = 3\lambda$ while $f(x_1) = 0$ outside this interval. Where h is the parameter which determines the roughness level. All the parameters except the surface roughness are chosen as the same in the first example illustrated in Figure 4.11. Figure 4.13 demonstrates the scattering widths for three different values of h. One can obviously see that the level of roughness has a strong effect on the scattered field from buried objects.

In Figure 4.14 the scattering widths corresponding three different conductivities in the case of a circular cylinder whose dielectric permittivity is $\varepsilon = 2.25\varepsilon_0$ are plotted. The cylinder is buried in a material having electromagnetic parameters $\varepsilon_2 = 4\varepsilon_0$ and $\sigma_2 = 2.22.10^{-5}(S/m)$. The surface has a roughness of $f(x_1) = 0.3\lambda e^{-\frac{x}{3}-\frac{|x|}{3}\frac{|x|}{5}}cos(\frac{3\pi x_1}{2\lambda})$ in the interval $(-3\lambda, 3\lambda)$ like in preceding example. As is expected that the conductivity affects scattered field in a strong way.

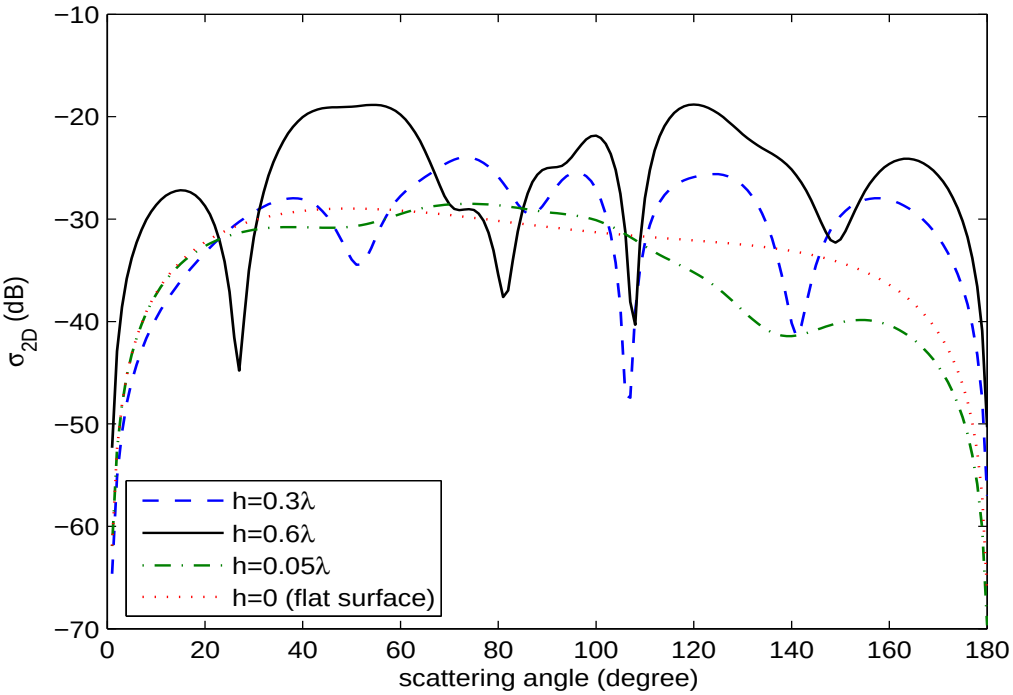


Figure 4.13: Scattering widths corresponding to buried circular cylinder in the existence of three different levels of the roughness.

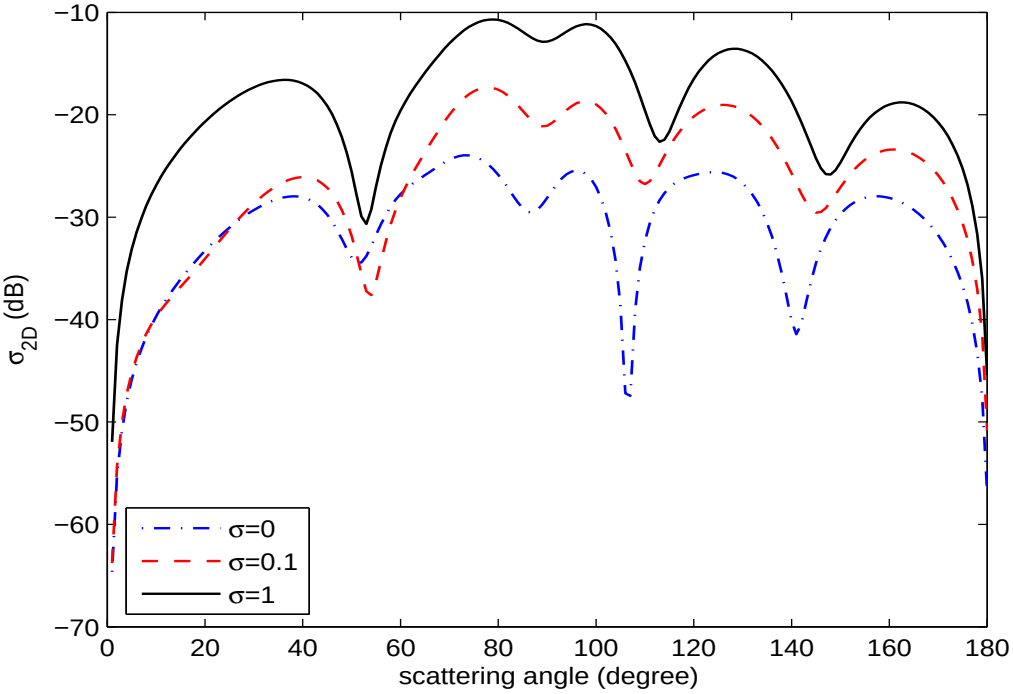


Figure 4.14: Scattering widths corresponding three different conductivities of the buried object.

In Figure 4.15 the effect of the incidence angle of the plane wave on the scattering width is depicted for the same problem as in the previous one.

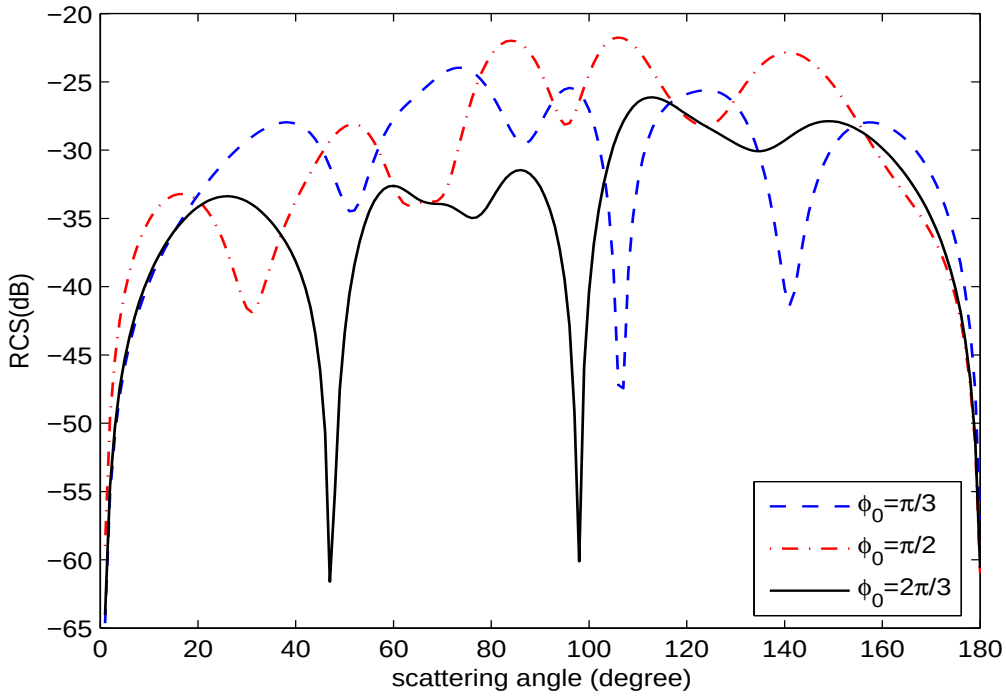
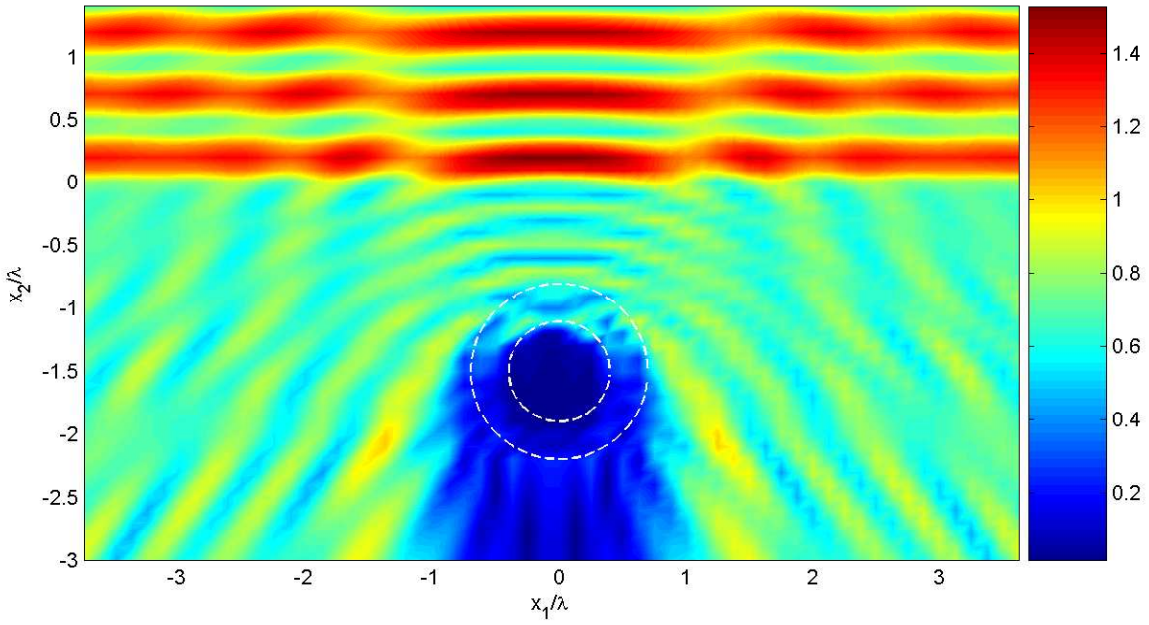
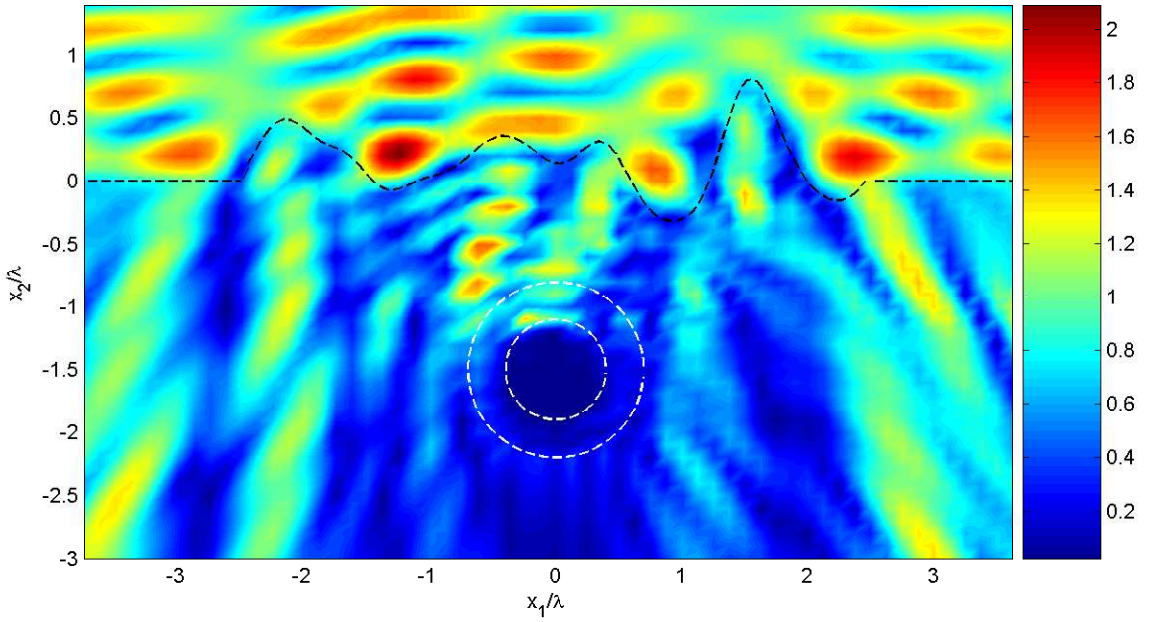


Figure 4.15: Scattering widths corresponding three different incidence angles of the plane wave.

To see the effect of roughness to the total field we compare the total fields due to a cylindrical body composed of two concentric circular cylinders buried in a dry soil with flat and rough interface. The electromagnetic parameters of the inner and outer regions of the body are chosen as $\varepsilon = 16\varepsilon_0$, $\sigma = 2.13(S/m)$ and $\varepsilon = 9\varepsilon_0$, $\sigma = 0$, respectively. Two-dimensional variation of the amplitude of the total field in a rectangular region in the case of flat interface for the normal incidence is illustrated in Figure 4.16a, while Figure 4.16b shows the amplitude of the total field for random rough interface with a roughness $\sigma_r = 0.3\lambda$, $\ell_c = 0.4\lambda$ and $L = 5\lambda$. In the numerical simulations the object is divided into 612 rectangular cells with sizes $\frac{\lambda}{20} \times \frac{\lambda}{20}$. The same cell sizes are also used in buried object modeling of the roughness for calculation of $\bar{G}(\mathbf{x};\mathbf{y})$. The significant interference between the object and the rough interface as well as the effect of the roughness to the total field can easily be observed from Figure 4.16b.



(a)



(b)

Figure 4.16: The magnitude of the total electric field in the existence of two concentric circular cylinders buried beneath (a) a flat air-dry soil surface and (b) a random rough surface of $\sigma_r = 0.3\lambda, \ell_c = 0.4\lambda$ and $L = 5\lambda$

The near field variation of the amplitude of total electric field for two elliptical cylindrical objects with electromagnetic parameters $\varepsilon = 16\varepsilon_0$, $\sigma = 2.13(S/m)$ buried in dry soil under a quite long and rapidly varying random rough interface with $\sigma_r = 0.4\lambda$, $\ell_c = 0.3\lambda$, $L = 18\lambda$ is demonstrated in Figure 4.17. The cell sizes for both Green's function and the objects are chosen as $\frac{\lambda}{20} \times \frac{\lambda}{20}$.

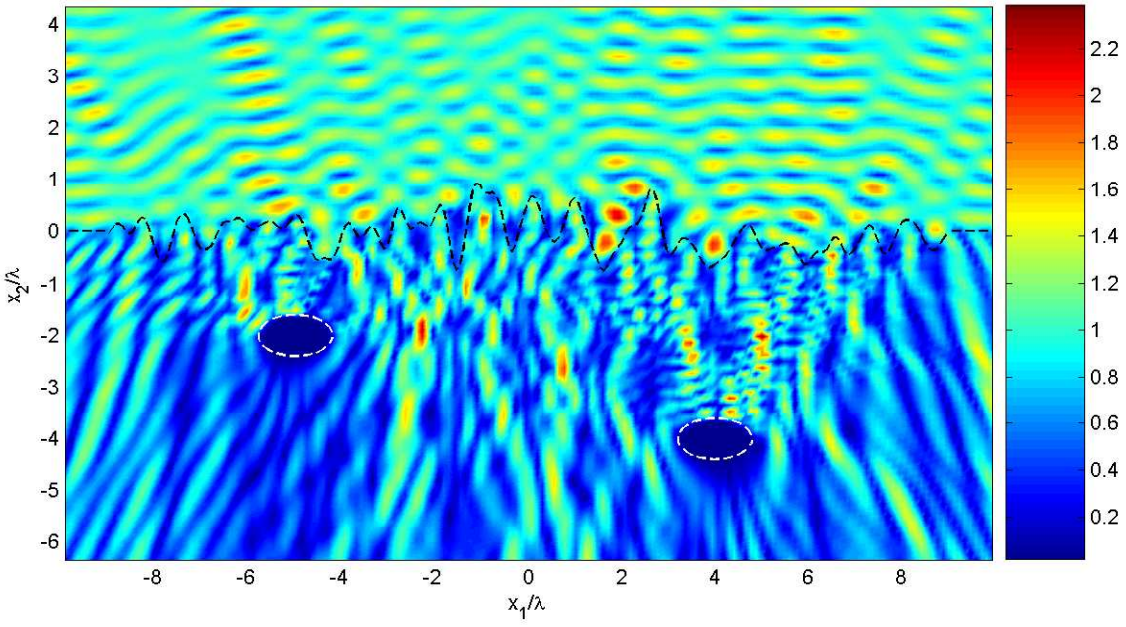


Figure 4.17: The magnitude of the total electric field in the existence of elliptical objects with same cross-sections, buried under a random rough interface with $\sigma_r = 0.4\lambda, \ell_c = 0.3\lambda$ and $L = 18\lambda$

Figure 4.18 is the same plot for a body with rectangular cross section embedded in dry soil with a random ground roughness $\sigma_r = 2.2\lambda$, $\ell_c = 0.3\lambda$ and $L = 10\lambda$. Note that in this example the roughness of the surface is quite large and is in the order of those given in [40].

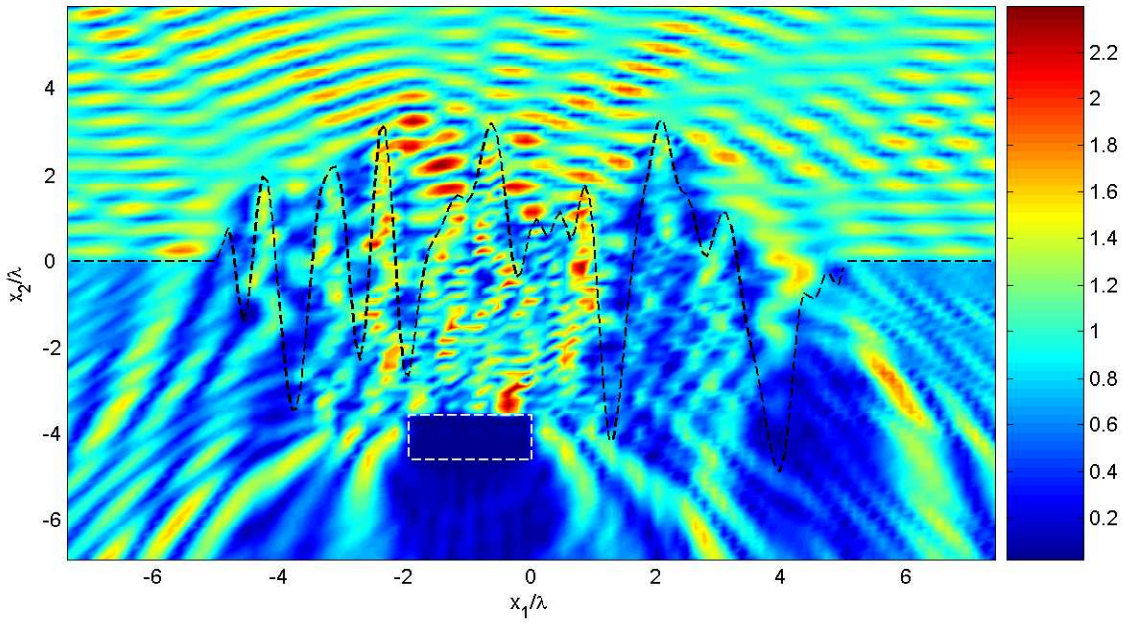


Figure 4.18: The magnitude of the total electric field in the existence of a rectangular object buried under a random and highly rough surface with $\sigma_r = 2.2\lambda, \ell_c = 0.3\lambda$ and $L = 10\lambda$

To show the interaction between objects of different shapes and materials we consider the case of three buried objects having kite, circular and drop shaped cross sections and made of materials with electromagnetic parameters $(\varepsilon = 20\varepsilon_0, \sigma = 3(S/m))$, $(\varepsilon = 20\varepsilon_0, \sigma = 0.5(S/m))$ and $(\varepsilon = 20\varepsilon_0, \sigma = 1(S/m))$, respectively. The bodies are buried in dry soil under a rough interface with $\sigma_r = 0.4\lambda$, $\ell_c = 0.5\lambda$ and $L = 8\lambda$. The variation of the magnitude of the total electric field in a rectangular domain containing the surface and the objects for the normal incidence case is given in Figure 4.19. It has been used same cell sizes as in the previous example for both Green's function and the objects. It has been observed that the computational cost of the method does not vary from objects having simple cross-sections (circular, rectangular, etc.) to more complex ones.

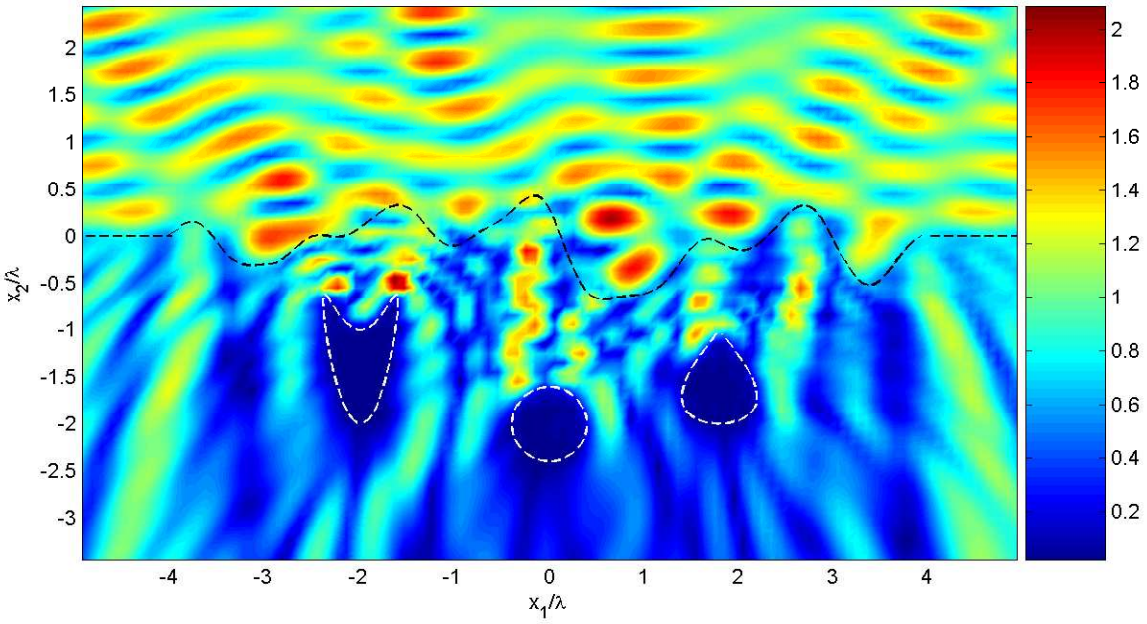


Figure 4.19: The magnitude of the total electric field in the existence of three different shaped objects having different conductivities buried under a rough interface with $\sigma_r = 0.4\lambda, \ell_c = 0.5\lambda$ and $L = 8\lambda$

5 CONCLUSIONS

A new method, which is called *buried object approach*, to solve the scattering problems related to both rough surfaces and bodies buried under a rough surface is presented. The method is based on the assumption that the irregularities of a rough surface are cylindrical bodies embedded in a two half-space media with planar boundary. This allows one to formulate the scattering problem connected with rough surfaces as a scattering of electromagnetic waves from cylindrical bodies buried in a two half-spaces medium with planar interface, which can be solved through an application of the MoM.

On the other hand, the scattering problems related to buried objets can be solved through MoM when the Green's function of the background medium is known. Whereas the determination of the Green's function of a layered media with rough interface constitutes a difficult and interesting problem. The *buried object approach* can also be used to this aim. In such a case one solve rough surface scattering problem for the cylindrical wave incidence through the *buried object approach*.

In the application of MoM, both bodies buried in a two half-spaces media with rough interface, and the irregularities of the surface which are assumed to be cylindrical objects are divided into certain number of cells. Accuracy of the approximation requires cell sizes to be small and stability requires them to be large. The method is very effective and accurate as long as the irregularities of the rough interface from a flat one can be modeled as objects with sizes in the validity limits of MoM. From this we conclude that the method can be used for surfaces having a localized roughness. The roughness of the surfaces in the illustrative examples are much higher than those given in the open literature. When the size and length of the surface are increased, the number of unknowns become larger in which case the computational cost also increase.

Compared to the available methods the proposed method has the following advantages and disadvantages:

i) The method yields quite accurate results for highly rough surfaces. From this point of view it is more accurate than the methods based on physical optics and small perturbation approaches.

ii) The method allows one to obtain both near and far scattered fields in the lower and upper half-spaces for the arbitrary roughness.

iii) It does not require tapering on the incident wave as in the surface based-integral methods and allows one to solve the scattering problem for the plane, cylindrical or spherical wave incidences.

iv) The method is valid for lossy dielectric half-spaces whose conductivities are of order 10^{-2} or less.

vi) The computational cost of the method is generally higher than those surface based integral methods using MoM since the surface is modeled in terms of volumetric domains.

It should be noted that in the direct and inverse scattering problems related to the objects buried in a layered media with rough interfaces the determination of the Green's function of the background medium constitutes a very important problem. Due to the properties (ii) and (iii), the proposed method would be a very efficient tool to this aim.

Further works are directed to first reduce the computational cost of the method by using fast algorithm such as fast multi-pole method adopted to MoM and to extend the method to the 2D rough surfaces and 3D objects.

References

[1] Rice, SO., 1951, "Reflection of electromagnetic wave by slightly rough surfaces.", *Commun. Pure Appl. Math.*, 4, 351-378.

[2] Sanchezgil, JA. Maradudin, AA. and Mendez, ER., 1995, "Limits of validity of 3 perturbation theories of the specular scattering of light from one-dimensional, randomly rough, dielectric surfaces." *Journal of the Optical Society of America A-Optics Image Science and Vision*, 12, (7) 1547-1558.

[3] Soubret, A. Berginc, G. and Bourrely, C., 2001, "Backscattering enhancement of an electromagnetic wave scattered by two-dimensional rough layers." *Journal of the Optical Society of America A-Optics Image Science and Vision.*, 18, (11), 2778-2788.

[4] Fuks, IM. Voronovich, AG., 2000, "Wave diffraction by rough interfaces in an arbitrary plane-layered medium." *Waves in Random Media*, 10, (2), 253-272.

[5] Yarovoy, AG. de Jongh, RV. and Ligthart, LP., 2000, "Scattering properties of a statistically rough interface inside a multilayered medium", *Radio Science*, 35, (2), 455-462.

[6] Franceschetti, G. Iodice, A. Migliaccio, M. and Riccio, D., 1999, "Fractals and the small perturbation scattering model." *Radio Science*, 34, (5), 1043-1054.

[7] Chen, J. Lo, TKY. Leung, H. and Litva, J., 1996, "The use of fractals for modeling EM waves scattering from rough sea surface", *IEEE Transactions on Geoscience and Remote Sensing*, 34, (4), 966-972.

[8] Elfouhaily, T. Thompson, DR. Vandemark, D. and Chapron, B., 1999, "A new bistatic model for electromagnetic scattering from perfectly conducting random surfaces", *Waves in Random Media*, 9, (3), 281-294.

[9] Fitzgerald, RM. Maradudin, AA., 1994, "A reciprocal phase-perturbation theory for rough-surface scattering." *Waves in Random Media*, 4, (3), 275-296.

[10] Zhang, XD. Wu, ZS. and Wu, CK., 1997,"A phase perturbation technique for light scattering from randomly dielectric rough surfaces" *Chinese Physics Letters*, 14, (1), 32-35.

[11] Vazouras, CN. Yarovoy, AG. Moyssidis, MA. de Jong, RV. Fikioris, JG. and Ligthart, LP., 2000, "Application of perturbation techniques to the problem of low-frequency electromagnetic wave scattering from an air-ground interface", *Radio Science*, 35, (5), 1049-1064.

[12] Yarovoy, AG., 1996, "Small slope iteration technique for wave scattering from a rough interface of two media", *IEEE Transcations on Antennas and Propagation*, 44, (11), 1433-1437.

[13] Elfouhaily, T. Joelsen, M. Guignard, S. and Thompson, DR., 2003, "Analytical comparison between the surface current integral equation and the second-order small-slope approximation", *Waves in Random Media*, 13, (3), 165-176.

[14] Demir , MA. Johnson, JT., 2003, "Fourth-and higher-order small-perturbation solution for scattering from dielectric rough surfaces", *Journal of the Optical Society of America A-Optics Image Science and Vision*, 20, (12), 2330-2337.

[15] Johnson, JT., 1999, "Third-order small-perturbation method for scattering from dielectric rough surfaces", *Journal of the Optical Society of America A-Optics Image Science and Vision.*, 16, (11), 2720-2736.

[16] Warnick, KF. and Chew WC., 2001, "Numerical simulation methods for rough surface scattering", *Waves in Random Media*, 11, (1), R1-R30.

[17] R.T. Marchand and G.S. Brown, 1999," On the use of finite surfaces in the numerical prediction of rough surface scattering", *IEEE Transcations on Antennas and Propagation*, 47, (4), 600-604.

[18] Chan, CH. Tsang, L. and Li, Q., 1998, "Monte-Carlo simulations of large-scale one-dimensional random rough surfaces scattering at near-grazing incidence: Penetrable case", *IEEE Transcations on Antennas and Propagation*, 46, (1), 142-149.

[19] Chen, RM. West, JC., 1995, "Analysis of scattering from rough surfaces at large incidence angles using a periodic-surface moment method", *IEEE Transactions on Geoscience and Remote Sensing*, 33, (5), 1206-1213.

[20] Schwering, FK. Whitman, GM. and Triolo, AA., 2004, "New full-wave theory for scattering from rough metal surfaces- the correction current method: the TE-polarization case", *Waves in Random Media*, 14, (1), 23-60.

[21] Baudier, C. Dusseaux, R. Edee, KS. and Granet, G., 2004, "Scattering a plane wave by one-dimensional dielectric random rough surfaces-study with the curvilinear coordinate method", *Waves in Random Media*, 14, (1), 61-74.

[22] Chaikina, EI. Navarrete, AG. Mendez, ER. Martinez, A. and Maradudin, AA., 1998, "Coherent scattering by one-dimensional randomly rough metallic surfaces", *Applied Optics*, 37, (6), 1110-1121.

[23] Yang, TQ. Broschat, SL., 1992, "A comparison of scattering model results for 2-dimensional randomly rough surfaces", *IEEE Transcations on Antennas and Propagation*, 40, (12), 1505-1512.

[24] Millet, FW. and Warnick, KF., 2004,"Validity of rough surface backscattering models", *Waves in Random Media*, 14, (3), 327-347.

[25] S.F. Mahmoud, S.M. Ali and J. R. Wait, 1981, "Electromagnetic scattering from a buried cylindrical inhomogeneity inside a lossy earth", *Radio Science*, Vol.16, No.6, pp: 1285-1298, Nov.-Dec.

[26] D.A. Hill, 1988, "Electromagnetic scattering by buried objects of low contrast", *IEEE Trans. Geosci.and Remote Sensing*, Vol.26, No.2, pp: 195-203.

[27] G.A. Ellis and I. C. Peden, 1995, "An analysis technique for buried inhomogeneous dielectric objects in the precence of an air-earth interface", IEEE Trans. Geosci.and Remote Sensing, Vol.13, No.3, pp: 535-540.

[28] M.D. Vico, F. Frezza, L. Pajewski and G. Schettini, 2005, "Scattering by a finite set of perfectly conducting cylinders buried in a dielectric half-space:a spectral-domain solution", *IEEE Transaction On Antennas an Propagation*, Vol.53, No.2, pp: 719-727.

[29] P.G. Cottis and J.D. Kanellopoulos, 1992, "Scattering of electromagnetic waves from cylindrical inhomogeneities embedded inside a lossy medium with sinusoidal surface", *J. Electromagnetic Waves and Appl.*, Vol.6, No.4, pp: 445-458.

[30] P.G. Cottis, C.N. Vazouras, C. Kalamatianos and J.D. Kanellopoulos, 1996, "Scattering of TM waves from a cylindrical scatterer buried inside a two-layer lossy ground with sinusoidal surface", *J. Electromagnetic Waves and Appl.*, Vol.10, pp: 1005-1021.

[31] D.E. Lawrance and K. Sarabandi, 2002, "Electromagnetic scattering from a dielectric cylinder buried beneath a slightly rough surface", *IEEE Trans. on Antennas and Prop.*, Vol. 50, No. 10, pp. 1368-1376.

[32] T. Chiu and K. Sarabandi, 1999, "Electromagnetic scattering interaction between a dielectric cylinder and slightly rough surface", *IEEE Trans. on Antennas and Prop.*, Vol. 47, pp. 902-913,.

[33] J. T. Johnson, 2001, "Thermal emission from a layered medium bounded by a slighly rough interface", *IEEE Trans. Geosci.and Remote Sensing*, Vol.39, pp: 368-378.

[34] J. T. Johnson and R.J. Burkholder, 2001, "Coupled canonical grid/discrete dipole approach for computing scattering from objects above or below a rough interface", *IEEE Trans. Geosci.and Remote Sensing*, Vol.39, No.6 pp: 1214-1220.

[35] J. T. Johnson and R.J. Burkholder, 2004, "A study of scattering from an object below a rough surface", *IEEE Trans. Geosci.and Remote Sensing*, Vol.42, No. 1 pp: 59-66,.

[36] A. W. Morgenthaler and C.M. Rappaport, 2001, "Scattering from lossy dielectric objects buried beneath randomly rough ground: validiting the semi-analytical mode matching algorithm with 2-D FDFD", *IEEE Trans. Geosci.and Remote Sensing*, Vol.39, No. 11 pp: 2421-2428.

[37] J. Q. He, T. J. Yu, N. Geng and L. Carin, 2000, "Method of moment analysis of electromagnetic scattering from a general three-dimensional dielectric target embedded in a multilayered medium", *Radio Science*, Vol.32, pp: 305-313.

[38] M. El-Shenawee, 2003," Scattering From Multiple Objects Buried Beneath Two-Dimensional Random Rough Surface Using the Steepest Descent Fast Multipole Method", *IEEE Trans. on Geosience and Remote Sensing*, Vol. 51, No. 4.

[39] M. El-Shenawee and C. Rappaport, 2003, "Electromagnetic scattering interference between two shallow objects buried under 2-D random rough surfaces", *IEEE Microwave and Wireless Componets Letters*, Vol.13, No. 6 pp: 223-225.

[40] A. Madrazo and M. Nieto-Vesperinas, 1997, "Scattering of light and other electromagnetic waves from a body buried beneath a highly rough random surface ", *JOSA-A* , Vol.14 (8), pp:1859-1866.

[41] Sarabandi, K. and Chiu, T., 1997, " Electromagnetic scattering from slightly rough surfaces with inhomogeneous dielectric profiles", *IEEE Transcations on Antennas and Propagation* 45, (9), 1419-430.

[42] Yu, T. and Carin, L., 2002, " Parallel Extended-Born analysis of electromagnetic scattering from 3-Dimensional sub-rough surface targets, *IEEE AP Society International Symposium*, Vol.4, 260-263.

[43] A. Ishimaru, J.D. Rockway and Y. Kuga, 2000, "Rough surface Green's function based on the firs-order modified perturbation and smoothed diagram method", *Waves Random Media*, 10, pp: 17-31.

[44] Altuncu Y., Yapar A., Akduman I., "On the Scattering of Electromagnetic Waves by Bodies Buried in a Half-space with Locally Rough Interface", *IEEE Trans.on Geoscience and Remote Sensing*, (in press).

[45] Altuncu Y., Akduman I., Yapar A., 2005, "On the Scattering of Electromagnetic Waves by Bodies Buried in a Half-space with Locally Rough Interface", *International Conference on Electromagnetics in Advanced Applications*, Torino-Italy.

[46] Nehari, Z., 1975, *Conformal Mapping*, Dover, New York.

[47] Tsang, L., Kong, JA. and Ding, KH., 2000, *Scattering of Electromagnetic Waves*, John Wiley and Sons, USA.

[48] M. Idemen, 1973, "Maxwell's Equations in the Sense of Distributions", *IEEE Trans. Antennas and Propagat.*, Vol.21 (5), pp.736-738.

[49] Felsen, LB. and Marcuvitz, N., 1973, *Radiation and Scattering of Waves*, Printice Hall, New Jersey.

[50] Harrington, RF., 1968, *Field Computation by Moment Methods*, Macmillan, Newyork.

[51] J.A. Richmond, 1965,"Scattering by a dielectric cylinder of arbitrary cross section shape", *IEEE Trans. on Antennas and Prop*, Vol.13 (3), pp.334-341.

[52] Ishimaru, A., 1991, *Electromagnetic Wave Propagation, Radiation and Scattering*, Prentice Hall, New Jersey.

[53] Chew, WC., Jandyala, V., Lu, CC., Michielssen, E., Song, JM. and Zhao, JS., 1997, "Fast multilevel techniques for solving integral equations in electromagnetics" *Asia Pacific Microwave Conference*, p.457-460.

BIOGRAPHY

Yasemin Altuncu was born in Sorgun, Turkey in 1975. She received the B.S and M.S degrees in electronic engineering from Erciyes University, Kayseri in 1996 and 1999, respectively. In 1998 she joined to electric electronics engineering department of Nigde University as a research assistant. She is currently working toward the Ph.D. degree at the Istanbul Technical University.